Paleo-valley infills record landscape response to late-Quaternary glacial/interglacial climate oscillations in the French western Alps

Vivien Mai Yung Sen, Pierre G Valla, Peter A van der Beek, François Lemot, Christian Crouzet, Gilles Brocard

Quaternary Science Reviews 331 (2024) 108632

Contents lists available at ScienceDirect

Quaternary Science Reviews

journal homepage: www.elsevier.com/locate/quascirev

Paleo-valley infills record landscape response to late-Quaternary glacial/interglacial climate oscillations in the French western Alps

Vivien Mai Yung Sen [a,b,*], Pierre G. Valla [a], Peter A. van der Beek [c], François Lemot [a,b], Christian Crouzet [a], Gilles Brocard [d]

[a] Institut des Sciences de La Terre (ISTerre), Univ. Grenoble Alpes, Univ. Savoie Mont Blanc, CNRS, IRD, Univ. Gustave Eiffel, Grenoble, France
[b] EDYTEM, Pôle Montagne, CNRS, Université Savoie Mont Blanc, Le Bourget-du-Lac, France
[c] Institut für Geowissenschaften, Universität Potsdam, Potsdam-Golm, Germany
[d] Maison de L'Orient et de La Méditerranée, Université Lyon 2, Lyon, France

ARTICLE INFO

Handling editor: Dr C. O'Cofaigh

Keywords:
Alluvial fills
Epigenic paleo-valleys
River profile reconstruction
Luminescence dating
Cosmic-ray exposure dating
Glacial/interglacial cycles
Incision/aggradation forcing
French western alps

ABSTRACT

Reconstructing mountainous landscape evolution throughout the Quaternary is challenging because of the poor long-term preservation of geomorphic records in a context of rapid surface dynamics and topographic rejuvenation. The Quaternary geomorphic evolution of the western European Alps has been strongly controlled by climatic oscillations between glacial and interglacial periods. Significant erosion and sediment remobilization during these glacial/interglacial cycles have left very few sedimentary archives to quantify the surface dynamics and paleo-environmental conditions within the mountain belt over the last hundreds of thousands of years. Alpine valleys within the periglacial zone are potential candidates to target long-term geological archives, since they may contain alluvial deposits that have been preserved from subsequent glaciations. In the Drac valley (French western Alps), three generations of paleo-valleys are preserved, each of which was filled with alluvial and lacustrine sediments in response to glacial damming downstream. The valleys were incised during subsequent times of glacial retreat, leading to the formation of epigenetic valleys. Detailed 3D mapping of the paleo-valleys was carried out using photogrammetric models to constrain their geometry. Mapping was combined with luminescence dating of alluvial deposits to reconstruct the temporal evolution of the Drac valley. This chronological framework, together with additional data from the literature, allowed us to quantitatively constrain the complex alluvial dynamics along the Drac river during the last ca. 230 ka. Poly-phased alluvial deposition occurred in the most recent paleo-valley between ca. 90 and 20 ka (i.e., from late MIS 5 to MIS 2) in a context of global climate cooling and major Alpine glaciation. Sediment infilling of the intermediate paleo-valley is dated at around 130 ka; i.e., during the late-glacial phase of the penultimate glaciation, at the abrupt warming transition between MIS 6 and MIS 5. Finally, the oldest paleo-valley was filled around 230 ka (during a sub-stage of MIS 7) probably in a cooling and glacial context. The overall alluviation pattern and chronology of the study area highlight the asynchronous and partially contrasting glacial dynamics between the different glacier systems (i.e., Drac, Bonne and Romanche/Isère glaciers) within the Ecrins-Pelvoux massif of the French western Alps.

1. Introduction

Since the seminal work of Penck and Brückner (1909), fluvio-glacial deposits have been important markers of oscillating glacial-interglacial climate variations and associated paleo-environmental conditions in mountainous settings. However, the fluvial dynamics in response to glacial fluctuations (i.e., advances and retreats) can be complex (Vandenberghe, 2008), as these dynamics are driven by synchronous or asynchronous changes in water and/or sediment flux, base-level variations, blocking of rivers by advancing ice masses, or combinations of these processes (Cordier et al., 2017 and references therein). Thus, the timing of fluvial sediment deposition with respect to global climatic variations (e.g., Bull, 1991; Bridgland and Westaway, 2008) or, more specifically, glacial advances and retreats (e.g., Pinter et al., 1994; Pan et al., 2003) may vary significantly from one site to another. Moreover, it is becoming increasingly clear that glacial fluctuations themselves

* Corresponding author. Institut des Sciences de la Terre (ISTerre), Univ. Grenoble Alpes, Univ. Savoie Mont Blanc, CNRS, IRD, Univ. Gustave Eiffel, Grenoble, France.
E-mail address: vivien.mai-yung-sen@univ-smb.fr (V. Mai Yung Sen).

https://doi.org/10.1016/j.quascirev.2024.108632
Received 13 December 2023; Received in revised form 14 March 2024; Accepted 21 March 2024
Available online 30 March 2024

may be strongly asynchronous, both globally (Gillespie and Molnar, 1995; Hughes et al., 2013) and regionally (e.g., Zech et al., 2008; Owen and Dortch, 2014; Monegato et al., 2017; Gribenski et al., 2021), depending on spatial and temporal variations in the climatic drivers. Much of the continental record of glacial-interglacial climate variations is contained in markers located in the forelands of mountain belts (e.g., Heiri et al., 2014); records from within the mountain belt have a strongly reduced preservation potential prior to the Last Glacial Maximum (LGM, 26.5–19.0 ka; Clark et al., 2009) due to glacial reoccupation and associated rapid erosion. However, more proximal deposits may be more sensitive proxys of higher-frequency climatic oscillations and associated geomorphic responses (e.g., Wickert and Schildgen, 2019; McNab et al., 2023), whereas such signals are potentially blurred in more distal deposits from the foreland.

The modern topography of the European Alps, characterized by high peaks and deeply incised valleys, was significantly affected by glaciations (e.g., Valla et al., 2021; Ivy-Ochs et al., 2022 and references therein). Although the first Alpine glaciations may date from the end of the Pliocene and the Early Pleistocene (Ehlers and Gibbard, 2004; Preusser et al., 2011), major and unambiguously dated glaciations, which profoundly marked the relief as well as sedimentation in the peripheral basins, occurred from the Middle Pleistocene transition (MPT; ca. 0.9 Ma) onward (Muttoni et al., 2003; Haeuselmann et al., 2007; Valla et al., 2011; Knudsen et al., 2020; Dieleman et al., 2022). From then on, the Alps have experienced strong oscillations between glacial and interglacial periods, driven by ~100 ka climatic cycles (Lisiecki, 2010). Modelling of Alpine glacier dynamics shows their high sensitivity to climatic forcing, resulting in numerous glacial advances to the foreland, followed by glacial retreats, on relatively short time scales (~1–10 ka; Seguinot et al., 2018). These dynamics led to rapid changes in the zonal distribution of dominant surface processes (i.e., glacial, glaciolacustrine, fluvio-glacial and fluvial) as well as significant changes in local base levels and the loci of erosion and sedimentation (Seguinot and Delaney, 2021).

Fluvial deposits and terraces are widespread along rivers of the French western Alps, both within the mountain belt and in its foreland, and are generally interpreted as being climatically controlled (e.g., Mandier, 1984; Starkel, 2003). However, quantitative chronological constraints are available for relatively few of these deposits, and their correlation is challenging due to the variable controls on deposition and incision (e.g., Brocard, 2002). Documented fluvial incision rates for western Alpine rivers vary widely: in general, extremely rapid (up to > 1 cm/yr) transient post-glacial incision rates in glacially perturbed rivers (e.g., Brocard et al., 2003; Valla et al., 2010; Rolland et al., 2017) are superimposed on long-term (10^5–10^6 yr) rates of ~0.5–1.0 mm/yr (Brocard et al., 2003; Petit et al., 2017; Cardinal et al., 2022). The latter rates are consistent with regional present-day uplift rates measured with geodetic techniques (Nocquet et al., 2016; Sternai et al., 2019) and are interpreted as recording a regional isostatic response to locally rapid erosion within the core of the Alps, together with some deep-seated geodynamic uplift mechanism, possibly related to slab detachment and/or asthenospheric upwelling (Champagnac et al., 2007, 2008; Nocquet et al., 2016; Sternai et al., 2019).

Beyond the LGM, the role of the successive glacial-interglacial phases in driving incision of the Alpine valleys remains poorly constrained, as are the respective contributions of glacial and fluvial processes to the observed incision (e.g., Leith et al., 2018; Valla et al., 2021). A quantitative assessment of landscape development throughout successive glacial – interglacial stages is challenging because of the limited preservation of sedimentary and geomorphological archives that predate the LGM in the Alpine massifs. In the piedmonts of the European Alps, frontal moraine complexes and periglacial deposits are preserved in the Swiss (Preusser et al., 2011), French (Monjuvent, 1978; Mandier, 2003; Roattino et al., 2021) and Italian (Gianotti et al., 2008, 2015; Kamleitner et al., 2022) forelands. These archives allow reconstructing maximum glacial extents and chronologies, in particular for the more recent glacial phases. However, they only constrain the maximum glacial extents in the piedmonts and mostly pertain to the LGM around 20–30 ka (Ivy-Ochs et al., 2018; Gribenski et al., 2021; Roattino et al., 2023); they do not reflect glacial dynamics and associated landscape development over successive glaciations within the Alpine chain itself. Constraining the latter requires analysing rare geomorphological or sedimentary archives from within the Alpine massifs that have been at least partially preserved from subsequent erosion. Glacial overdeepenings around and within the Alpine chain (e.g., Nicoud et al., 2002; Preusser et al., 2010; Magrani et al., 2020) offer precious sedimentary archives to assess erosional and environmental conditions over subsequent glaciations (Anselmetti et al., 2022); however, their access and detailed investigation are logistically challenging, and they provide information specific to (sub-)glacial processes in major Alpine valleys and forelands (e.g., Nicoud et al., 2002; Dehnert et al., 2012; Schwenk et al., 2022; Gegg et al., 2023).

Here, we focus on the fluvio-glacial record of the Drac valley, located in the French western Alps at the margin of major LGM glaciers (Fig. 1). Extensive Quaternary glacial, fluvial and lacustrine deposits have been mapped and described in detail in the Drac valley (Monjuvent, 1973, 1978; Brocard, 2002; Bièvre and Crouzet, 2021), linked to the unique fluvio-glacial dynamics of this valley (see below). Among these deposits, the Drac paleo-valleys are remarkable Quaternary archives: at least three generations of these epigenetic valleys and their alluvial fills provide a record of repeated fluvial aggradation and incision over several Pleistocene glacial/interglacial cycles (Monjuvent, 1978; Brocard, 2002). We employ 3D mapping of the paleo-valleys from newly acquired photogrammetric models, together with feldspar luminescence dating of the alluvial fills and reassessment of previously published cosmogenic-nuclide exposure ages, to obtain new spatial and chronological constraints on these deposits.

2. Study area

The Drac valley is located in the French western Alps and follows a mainly north-westerly course from its source in the southern Pelvoux massif to its junction with the Isère River near the city of Grenoble (Fig. 1). The Drac valley separates the “Sub-alpine” Vercors and Dévoluy massifs, consisting mainly of Jurassic-Cretaceous calcareous sedimentary rocks, to the west from the Pelvoux “External Crystalline Massif”, exposing crystalline basement, to the east. The Drac valley contains large volumes of Quaternary sediments (Figs. 2 and 3) with a complex stratigraphy and geometry. The Quaternary deposits of the Drac valley have been studied since the middle of the 19th century (Lory, 1860) but only with the work of Monjuvent (1973, 1978) has a detailed stratigraphic description become available. These up to 400-m thick sediment accumulations can be explained by the paleogeographic setting of the Drac basin during Pleistocene glaciations. The lack of active tectonic structures within the Drac catchment, as well as the lack of evidence for large valley-blocking landslides, rules out a tectonic or landslide origin for these extensive deposits (Monjuvent, 1973, 1978; Brocard, 2002).

During the last glacial cycle, the Drac valley was located at the margin of the large Isère-Romanche glacier system and was fed by the Drac, Séveraisse and Bonne glaciers upstream (Fig. 1). During glacial maxima, the Durance glacier also fed the Drac watershed through transfluence from the South. The MIS 6 glacial period was the last time when the Drac watershed was totally glaciated (Monjuvent, 1973, 1978). During the LGM, the Drac valley was only partially glaciated, in contrast to its eastern tributaries and other large Alpine valleys. The downstream part of the Drac was dammed by a southward-flowing tongue of the Isère/Romanche glacier, which led to a base-level rise of ~500 m, blocking of the river, and the formation of the Trièves paleolake (Monjuvent, 1973, 1978). Similarly, the terminal tongue of the Bonne glacier obstructed the middle course of the Drac, thus forming the Beaumont paleolake (Fig. 1). The rise of the local base level by several hundreds of meters promoted sediment aggradation in the Drac valley

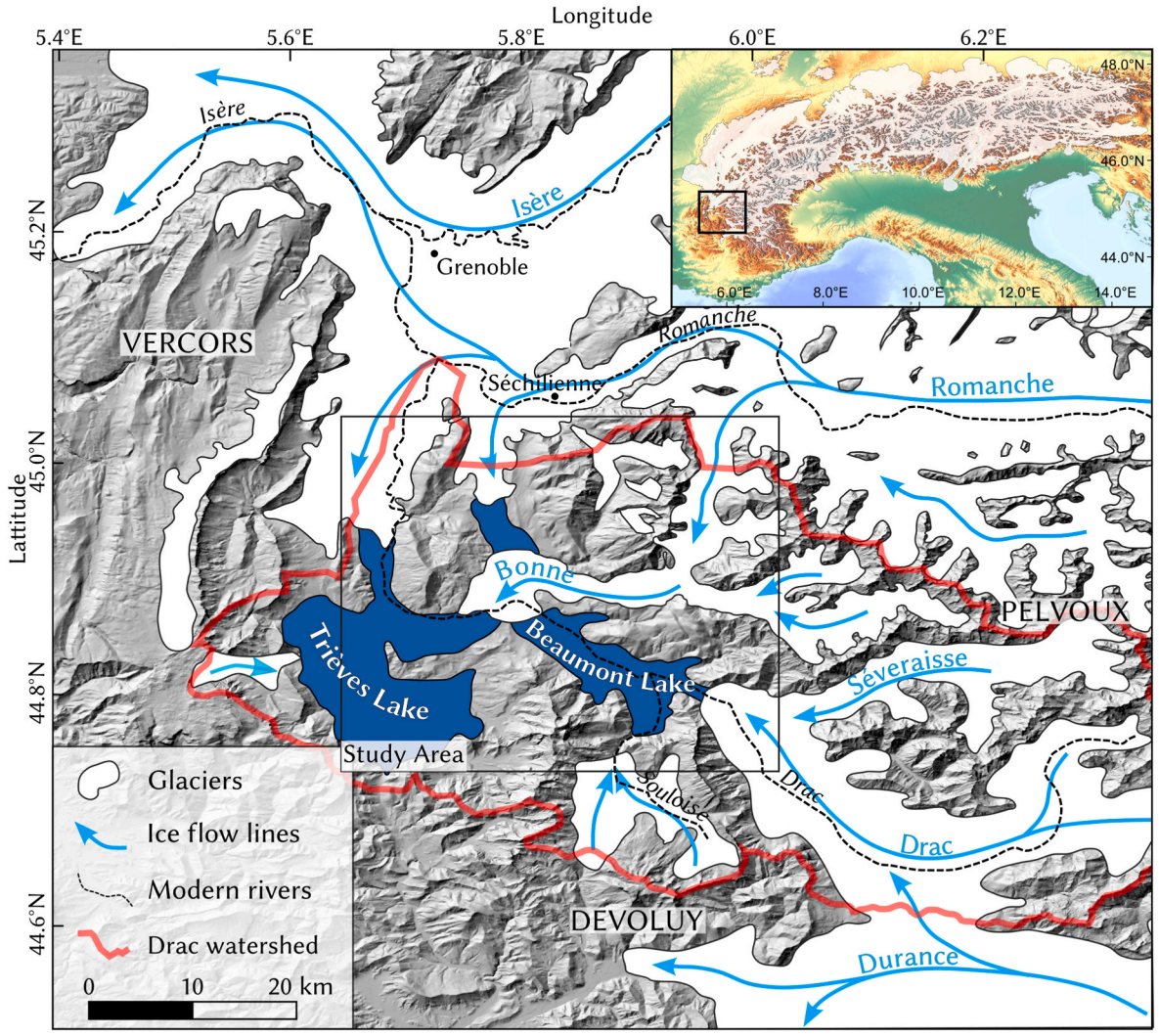

Fig. 1. Glacier extent, ice flow lines and glacially dammed lakes in the Drac valley during the Last Glacial Maximum (MIS 2) (after Monjuvent, 1978; Coutterand, 2010). Base map: shaded 25-m resolution DEM from the Institut Géographique National (IGN BD Alti 25). Dashed black lines indicate modern Alpine rivers. The inset shows the location (box) in the European Alps and the maximum extent of LGM glaciers (after Ehlers and Gibbard, 2004). The black frame shows the location of the study area (Fig. 2).

and the deposition of thick alluvial and lacustrine sequences (Fig. 2). Subsequent post-LGM glacier retreat led to a rapid base-level drop and ongoing epigenetic headward incision of the river, through both the fluvio-lacustrine deposits and the Mesozoic bedrock (mostly lower-Jurassic marls and limestones), by knickpoint retreat (Brocard et al., 2003). As a consequence, the modern Drac river is in a transient state, with a conspicuous propagating knickpoint separating a wide and open valley upstream from a relatively narrow and deep valley downstream (the modern knickpoint is located 10 km upstream of sample location Be5 in Fig. 2; Brocard, 2002).

Such glacial/interglacial oscillations and associated cyclical base-level rises and falls over the Pleistocene, together with cyclical variations in sediment supply, have led to a complex depositional sequence, which was described in detail by Monjuvent (1973, 1978). In particular, the middle course of the Drac is characterized by the presence of three generations of epigenetic paleo-valleys (V1, V2 and V3; Figs. 2 and 3), which are perched up to 200 m above the modern Drac riverbed. The characteristic V-shaped cross-profile of these paleo-valleys is evidenced where their course intersects the course of the modern Drac valley (Fig. 4). The paleo-valleys are filled with alluvial sediments composed of dm-size cobbles to boulders of fluvial to fluvio-glacial origin; we will denote these fills A1, A2 and A3, respectively. The alluvial clasts are composed of a mixture of magmatic, metamorphic and sedimentary rocks representative of the lithologies outcropping in the Drac catchment and similar to the sediments carried by the modern Drac river. At the Monteynard dam locality (Figs. 2 and 3), the floor of V1 is perched 200 m above the modern Drac river, whereas the floors of paleo-valleys V2 and V3 are located respectively 20 and 40 m above the present-day riverbed. In this downstream part of the study area, the alluvial deposits A2 and A3 are covered by laminated clays and silts of glacio-lacustrine origin deposited in the Trièves paleolake (Huff, 1974), with a maximum thickness of 250 m (Figs. 2 and 3). The age of these deposits has been constrained to between about 30 and 40 ka using bulk-clay ^{14}C dating (Bièvre and Crouzet, 2021). In the northern part of their mapped extent, these glacio-lacustrine deposits are covered by tills deposited by the Isère/Romanche glacier. In the central and southern parts of the study area, the glacio-lacustrine deposits transition up-section into deltaic deposits. These are topped by alluvial terraces, perched up to 300 m above the modern Drac riverbed. Cosmogenic-nuclide dating has provided late-to post-LGM ages for the abandonment of these high alluvial terraces (Brocard et al., 2003).

The geometry of the different paleo-valleys is well preserved and some are continuous along the current course of the Drac valley, allowing the reconstruction of the river-profile evolution and the

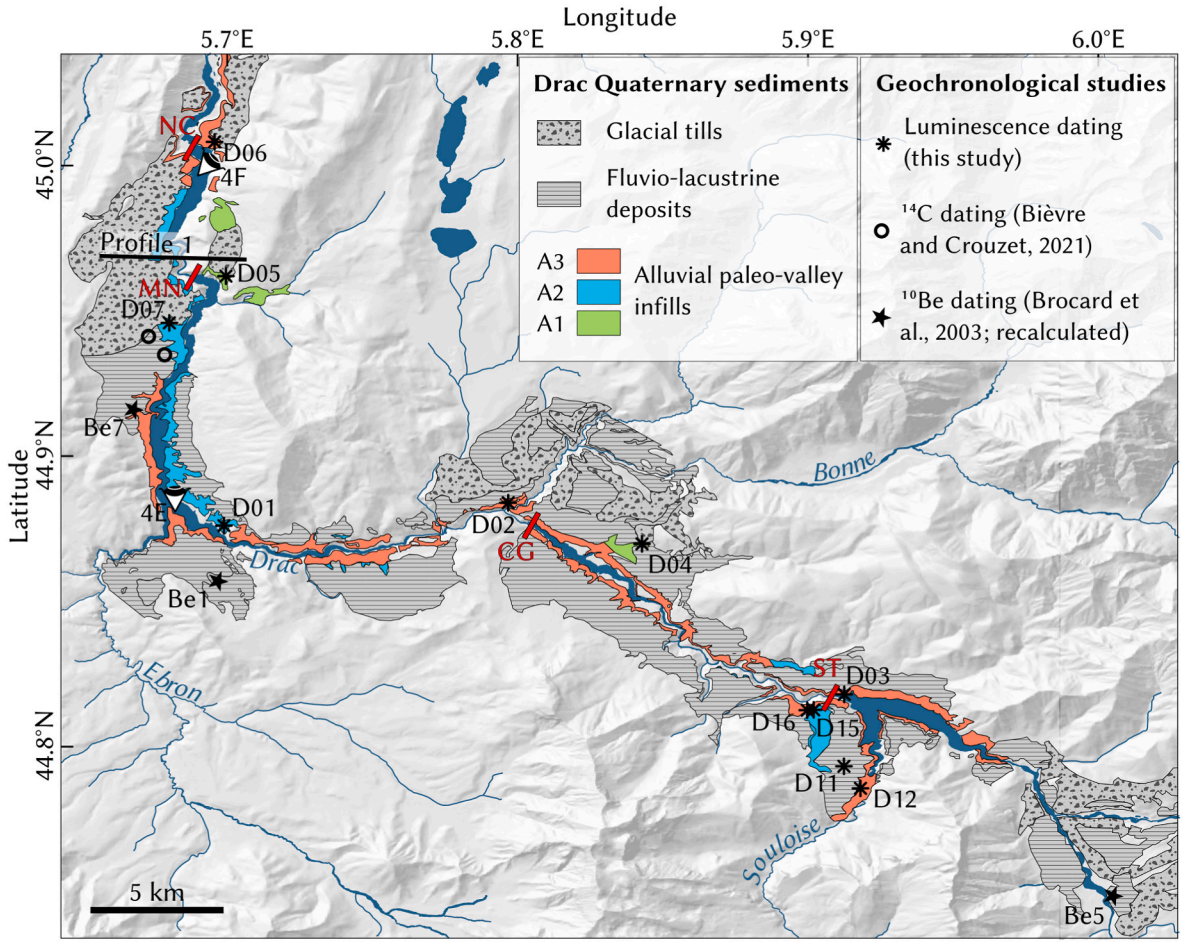

Fig. 2. Quaternary geological setting of the Drac valley, showing the spatial distribution of alluvial paleo-valley fills along the Drac river, covered by glacial and glaciolacustrine formations (from BRGM 1:50 000 scale geological maps; https://infoterre.brgm.fr/page/cartes-geologiques). Profile 1 shows the position of the cross-section shown in Figs. 3 and 9C. Base map: shaded IGN BD Alti 25-m resolution DEM. Black markers show locations of samples for feldspar luminescence dating and existing chronological data (see legend for details and references). Red bars are hydropower dams (NC: Notre-Dame-de-Commiers; MN: Monteynard; CG: Cognet; ST: Sautet). Eye symbols show locations of Fig. 4E and Fig. 4F.

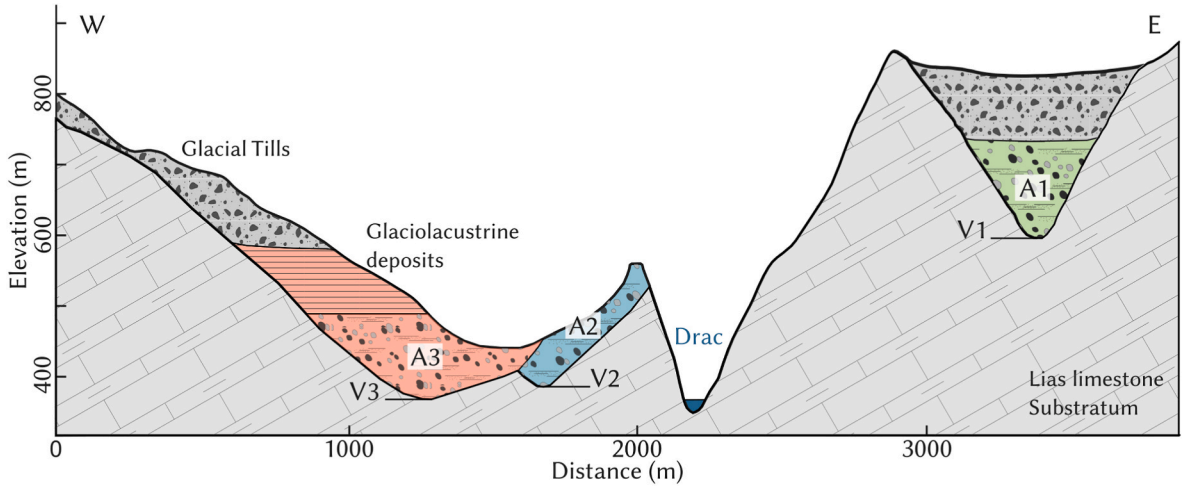

Fig. 3. Cross-section across the Drac valley at the Monteynard dam (see Fig. 2 for location) showing three generations of epigenetic paleo-valleys (V1, V2 and V3) perched at 200, 40 and 20 m above the modern Drac riverbed, respectively. The paleo-valleys are filled by coarse alluvial sediments (A1, A2, A3, in green, blue and red, respectively) covered by late-Pleistocene glacial tills (in grey) and glaciolacustrine deposits. See text for discussion. Modified from Monjuvent (1978).

morphological changes in connection with regional relief evolution under successive Alpine glaciations. The repeated incision and valley filling during the Pleistocene also affected the tributaries of the Drac trunk stream. In particular the Ebron, Bonne and Souloise valleys (Fig. 2) also contain alluvial deposits filling epigenetic paleo-valleys. Our study revisits the Drac paleo-valleys and their alluvial fills, which

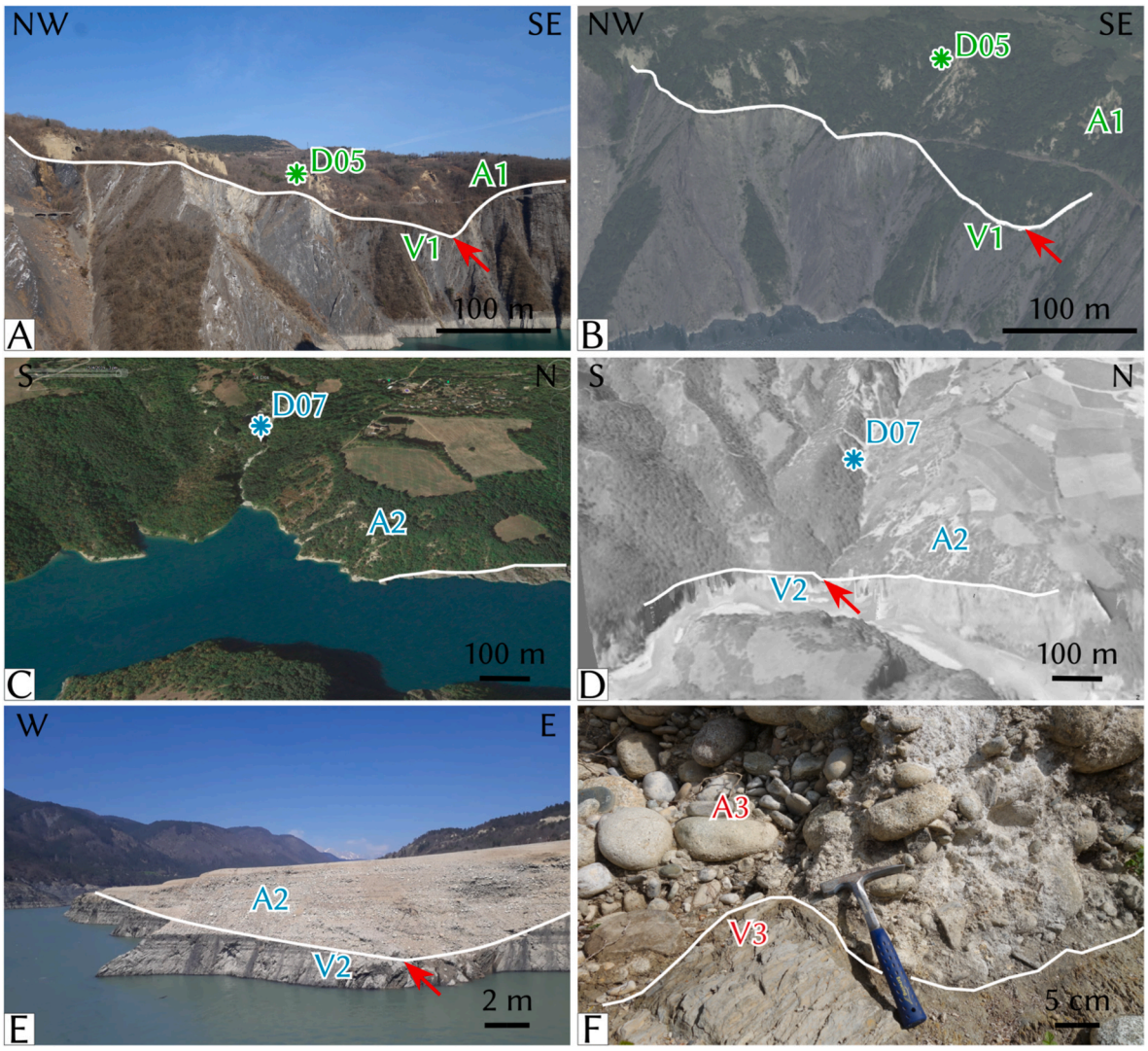

Fig. 4. 3D mapping of Drac paleo-valleys. The red arrows show the paleo-valley talwegs used to reconstruct the longitudinal profiles. White solid lines show paleo-valley sidewalls, and markers (D05 and D07) indicate sampling locations for feldspar luminescence dating. **A**. Photograph of the A1 paleo-valley at Monteynard dam. Note the characteristic V-shape of the base of the paleo-valley. **B**. Same outcrop as A on a 3D DTM constructed by photogrammetry from IGN aerial photographs dating from 2012. **C**. Present-day view (Google Earth) of paleo-valley A2, the talweg of which lies below the current level of the Monteynard reservoir. **D**. Same outcrop as C on a 3D DTM constructed by photogrammetry from IGN aerial photographs dating from 1956. **E.** A2 paleo-valley bottom and contact with Liassic limestone substratum just above the present-day level of the Monteynard reservoir. **F.** Contact between limestone bedrock and A3 fluvial cobbles. See Fig. 2 for location of panels E and F.

constitute key geological archives for reconstructing Pleistocene landscape dynamics in the French western Alps. New detailed 3D mapping of the Drac paleo-valleys allows a better reconstruction of their spatial relationships, and thereby constrain the long-term regional incision dynamics over the Middle-Late Pleistocene. We provide new chronological constraints on the valley fills to place their deposition within the climatic context of Pleistocene glacial-interglacial cycles and better understand the forcing mechanisms (variations in base-level and/or in sediment flux) on their deposition. More robust chronological constraints on the valley fills may also allow recording potential temporal disparities in the dynamics of large Alpine glaciers during the Pleistocene. The specific objectives of this study were to: (1) assess the incision and aggradation processes in this periglacial to glacial context; (2) determine the chronology of glacier fluctuations in this area; (3) derive long-term incision rates from the vertical offsets between the paleo-valley floors.

3. Methods

3.1. 3D mapping of modern and paleo-Drac river profiles

The study area corresponds to the middle course of the Drac, where the epigenetic gorges are best developed (Fig. 2). Within this steep and narrow reach, downstream of the main post-glacial retreating knickpoint, the profile of the Drac river shows numerous lithological knickpoints where the river crosses less erodible, thick-bedded limestones (Brocard et al., 2003). Some of these knickpoints were exploited in the 20th century as a natural base for the construction of four hydropower dams. The 50-km long reach of the present-day Drac in the study area therefore consists of a succession of reservoir lakes and steep bedrock-river sections, where the river flows on the Mesozoic substratum.

To characterize the spatial pattern of incision and aggradation of the Drac during Pleistocene glacial/interglacial cycles, we performed 3D mapping of the Drac paleo-valleys and present-day river profiles. To reconstruct the natural modern profile of the Drac, we used aerial

photographs of the valley taken before the hydropower reservoirs were flooded. We constructed digital terrain models (DTMs) from aerial imagery provided by the Institut National de l'Information Géographique et Forestière (IGN; https://www.ign.fr/). 173 IGN aerial photographs from 2012, covering the study area, were used to create a 3D photogrammetric model using Agisoft Photoscan software. We constructed another photogrammetric 3D model from 85 IGN aerial photographs taken in 1956, before the construction of the Notre-Dame-de-Commiers and Monteynard dams (cf. Fig. 2). Finally, 23 IGN aerial photographs from 1952 were used to reconstruct the valley topography under the Cognet reservoir (Fig. 2). The reservoirs on the 2012 DTM were then replaced by the valley topography from the 1952 and 1956 DTMs. No aerial imagery nor topographic maps including elevation contours were available from before the construction of the Sautet dam in 1935 (Pardé, 1935). We thus used three elevation points, estimated from field observations and historical documents, including a historical 19th century topographic map (https://www.geoportail.gouv.fr/donnees/carte-de-letat-major-1820-1866), as well as pre-dam maps and photographs of the Drac (Robert, 1926), to propose a first-order estimate of the Drac river profile under the Sautet reservoir. We extracted the modern river profile of the Drac from this topographic model using Topotoolbox (Schwanghart and Scherler, 2014).

To reconstruct the longitudinal profiles for the bases of the paleo-valleys, we mapped the stratigraphic contacts between the bedrock and the paleo-Drac alluvial deposits in 3D using literature data (Monjuvent, 1978; Brocard, 2002 and references therein), 1:50.000-scale geological maps of the French national geological survey BRGM (https://infoterre.brgm.fr/page/cartes-geologiques), a campaign of GPS acquisition and observations in the field (Fig. 4E and Fig. 4F), and digital mapping on the 3D DTMs constructed from aerial photographs (Fig. 4B and Fig. 4D). We projected the mapped contact points horizontally onto the modern Drac riverbed profile, using the smallest distance to the modern Drac riverbed (Fig. 5). Since the three paleo-valleys (V1, V2, and V3; Fig. 3) cannot be distinguished on a sedimentological or petrographical basis (i.e., both the lithological and grain-size characteristics of the three alluvial sediment fills are similar), we used a geometric criterion based on the elevation of the bottom and top of the paleo-valley infills to discriminate between the three paleo-valleys. We could easily distinguish V1 from V2 and V3 because V1 lies at significantly higher elevations than the other two paleo-valleys (Figs. 3 and 5). The distinction between V2 and V3 is more complicated because the alluvial fills of the two paleo-valleys overlap in elevation range. Three criteria were thus used to discriminate V2 from V3: (1) the paleo-profiles had to be continuous and consistent with a typical longitudinal river profile, i.e., continuous decrease in elevation downstream; (2) the profiles had to be consistent with the age of the alluvial deposits obtained by feldspar luminescence dating (see next section); (3) the top of the A2 fill is about 80 m higher than the top of the A3 fill (Fig. 3; Brocard, 2002).

3.2. Dating of paleo-valley alluvial sediment fills

To determine the depositional chronology of the mapped alluvial sediment fills, we conducted feldspar luminescence dating, focusing on sandy lenses within the alluvial deposits (Fig. 6). We specifically targeted the A1, A2 and A3 paleo-valley fills, for which no absolute dating was previously available. We extended our sampling area over the 50-km reach of the Drac river where the paleo-valley deposits were mapped (samples D01 to D07; Figs. 2 and 5A). We also sampled four additional locations on the high alluvial terraces of the Drac-Souloise confluence (samples D11 to D14; Figs. 2 and 5A) to better chronologically constrain the aggradation phases in this upstream location. Finally, we recalculated abandonment ages for terrace surfaces capping the most recent alluvial sediment fill. These were originally quantified using in-situ cosmogenic ^{10}Be profile data by Brocard et al. (2003); here we reassess these datasets using an updated ^{10}Be production rate, ^{10}Be half-life, and modelling approach (see below for details).

Sampling for luminescence analyses was carried out in at least 20-cm thick sandy lenses, to ensure sufficient bleaching before deposition and a homogeneous environmental dose rate. Samples were collected with opaque tubes to avoid any exposure of the sediment to daylight (Fig. 6) and additional alluvial material was collected around the sampled tube for dose-rate measurements. Samples were prepared under red-light conditions to prevent bleaching of the natural luminescence signal. The samples were washed in water and treated with HCl (32%) and H_2O_2 (30%) to remove carbonates and organic material, respectively. The 180-250-μm or 180-300-μm grain-size fractions (depending on samples) were separated by sieving (Table 1). The K-feldspar fractions were subsequently purified by density separations in LST heavy liquid at 2.70 and 2.58 g/cm$^{3.}$ 24 aliquots of each sample were mounted on stainless-steel discs using silicone spray for luminescence measurements (Lowick et al., 2015).

Luminescence measurements were performed on Risø TL/OSL DA-20 readers using internal ^{90}Sr/^{90}Y beta-sources at the Institute of Geology (University of Bern, Switzerland). Luminescence signals were detected using an EMI 9235QA photomultiplier tube in the blue region through a Schott BG-39 and L.O.T.-Oriel D410/30 nm filter combination. The single-aliquot regenerative-dose (SAR) protocol was followed for luminescence analysis (Murray and Wintle, 2000; Wallinga et al., 2000). A preheat treatment at 250 °C was applied during 60 s. The luminescence measurement cycles consisted of a first IRSL (Infra-Red Stimulation Luminescence) stimulation at 50 °C for 100 s (IRSL-50) followed by a second IRSL stimulation at 225 °C for 100 s (pIRIRSL-225). Measured luminescence signals were integrated over the first 1.2–11.2 s minus the last 90–100 s. For each aliquot, dose–response curves were constructed in Analyst software using combined exponential and linear fitting (Duller, 2015). Recycling ratios within 10% of unity and recuperation within 5% of the natural dose were used as acceptance criteria for the single-aliquot data. The suitability of the SAR protocol was confirmed by residual and dose-recovery tests (Wintle and Murray, 2006). For all samples, residual doses <3% of the natural dose and dose-recovery ratios within ±20% of unity were measured. Because of the better bleaching characteristics of the IRSL-50 signal (e.g., Colarossi et al., 2015) and given potential inherited pIRIRSL-225 signal for fluvio-glacial environments (e.g., Fuchs and Owen, 2008), we used only the IRSL-50 signal in the subsequent age determinations. Natural pIRIRSL-225 signals were mostly saturated for our samples, so only unsaturated natural IRSL-50 signals were used for the equivalent dose (De) interpolation from the dose–response curves. For samples with less than 20% De overdispersion (OD, Table 1 and Figs. S4–S5), a central age model (CAM) was applied (Galbraith et al., 1999; Galbraith and Roberts, 2012). For samples with OD > 20%, we applied a minimum age model (MAM; Galbraith et al., 1999; Galbraith and Roberts, 2012). Fading rates (Aitken, 1985) were measured on three aliquots of each sample used for De determination following Auclair et al. (2003). Final fading-corrected De values were calculated following the fading correction procedure of Huntley and Lamothe (2001), using the Luminescence R package (Kreutzer et al., 2012).

Calculation of the environmental dose rate for each sample was performed taking into account the burial depth measured in the field, the estimated water content, and the activities of U, Th and K (Table 1). About 200 g of sandy material was collected from the surrounding of each sample to determine water content and U, Th and K activities. The material was desiccated at 60 °C to enable quantification of water content. Significant dispersion in water content was measured between the samples (1–15%), leading us to question the representativeness of these field measurements. Therefore, a generic water content of 7 ± 3% was applied for the calculation of the environmental dose rate for all our samples. U, Th and K activities were measured using high-resolution gamma spectrometry in the Department of Chemistry and Biochemistry (University of Bern, Switzerland). Burial depths, generic water content, grain-size fractions used for luminescence analysis and radiogenic isotope activities were employed as inputs for final dose-rate

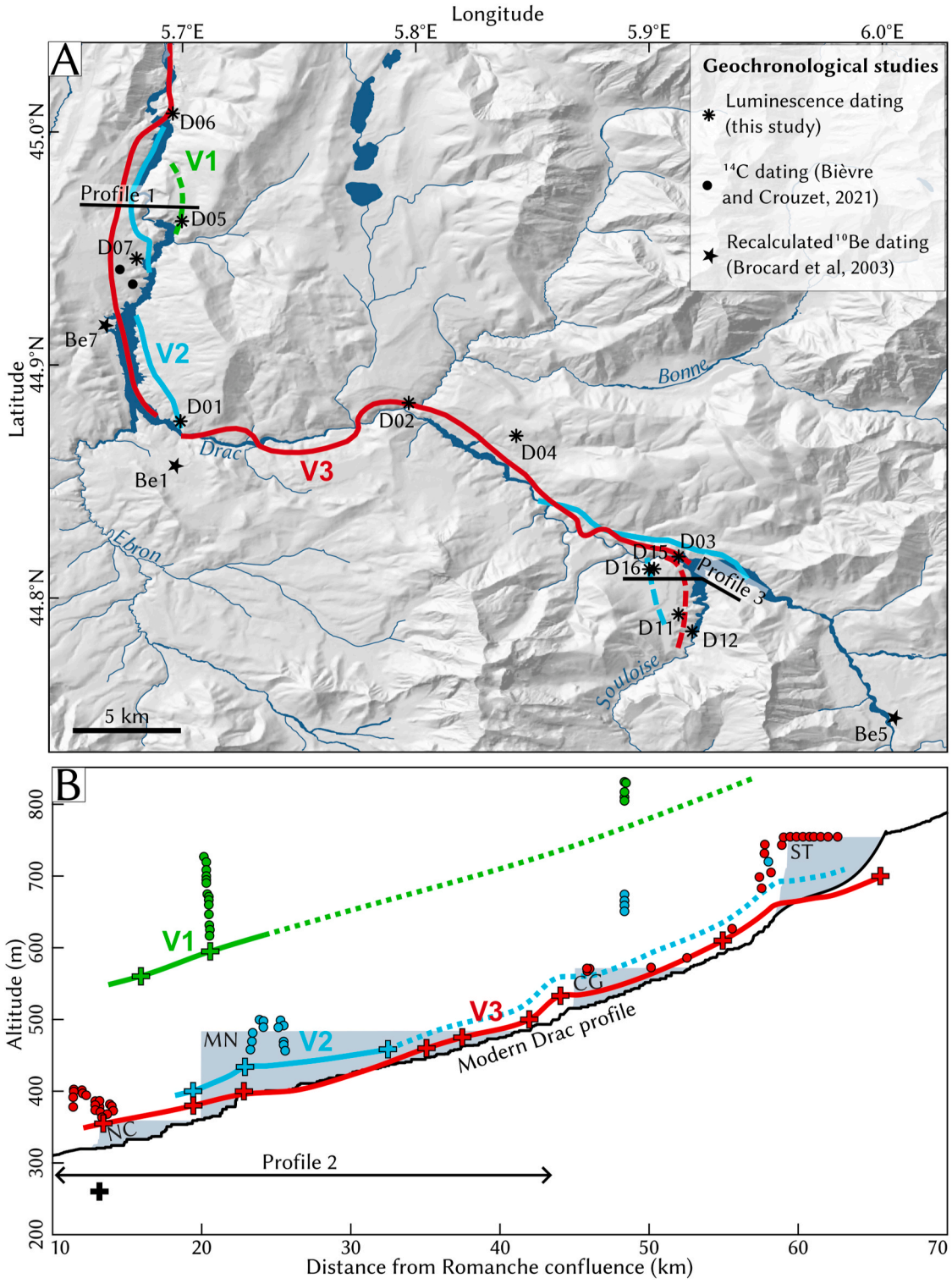

Fig. 5. Reconstruction of the Drac paleo-valleys V1, V2 and V3. **A.** Map of the Drac paleo-valleys. Profiles 1 and 3 refer to Fig. 9C and Fig. 9B, respectively. Paleo-valley V1 is only preserved above the Monteynard reservoir and in a few outcrops ~30 km upstream. V2 is almost continuous in the northern and southern part of the studied area, but not in the central part. V3 can be traced throughout the study area. The axes of the paleo-valleys are close to the modern Drac river axis. **B.** Reconstruction of the Drac paleo-valley profiles (paleo-valley bottoms and sidewalls) projected on the modern Drac longitudinal profile (black solid line) as a function of distance upstream of the Drac-Romanche confluence (cf. Fig. 1). Reservoirs are shown in light grey; abbreviations are as in Fig. 2. Alluvium-substratum contact points are classified between paleo-valleys A1, A2, and A3 based on the paleo-valley bottom elevation, maximum alluvial elevation, and luminescence dating results. The colored crosses are mapped paleo-valley bottoms, while colored dots are mapped paleo-valley sidewalls. These are used to constrain the maximum elevation of the paleo-valleys when the bottoms could not be mapped. The dotted lines are paleo-valley profile sections that are not constrained by available outcrops of paleo-valley bottoms. The black cross at the NC reservoir, in the downstream reach of the Drac, shows a borehole constraint on the elevation of the bedrock (Brocard, 2002) that can be attributed to either V2 or the modern Drac profile (no chronological constraint exists on the alluvial fill for this borehole). Profile 2 is shown in Fig. 9A.

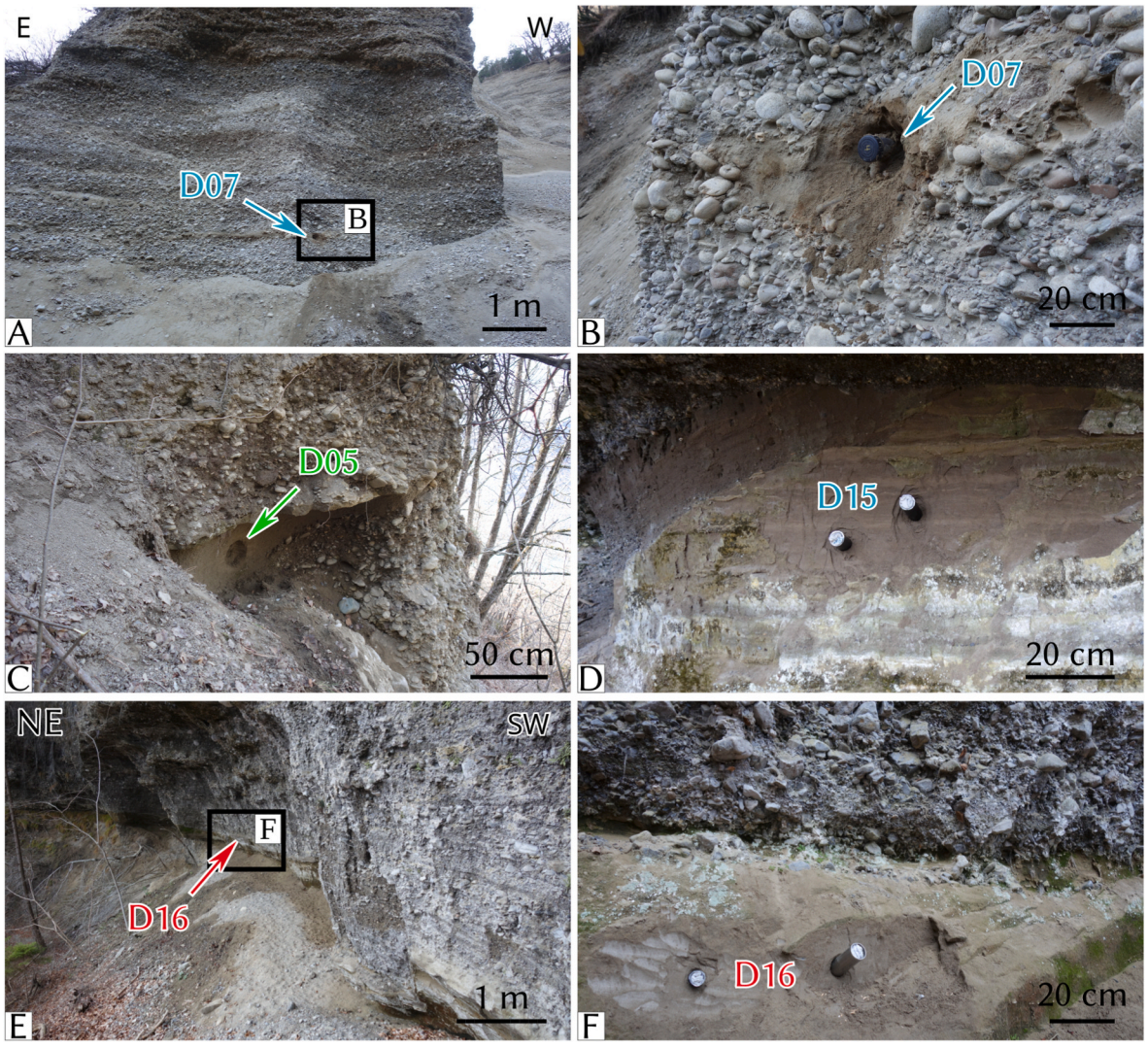

Fig. 6. Sampling sites (sandy lenses in the Drac and Souloise sediment fills) for feldspar luminescence dating. See Fig. 2 for location of the samples. **A-B-C.** Sampling sites D07 and D05, in sandy lenses of the paleo-Drac fills. **D-E-F.** Sampling sites D15 and D16, in sandy glacio-lacustrine layers of the paleo-Souloise fills. Whereas clasts are well rounded and polygenetic in the Drac fills, they are mostly angular and calcareous in the Souloise fills.

determination through the Dose Rate and Age Calculator (DRAC; Durcan et al., 2015).

We also used chronological constraints from ^{10}Be exposure dating on alluvial terraces that developed on top of the paleo-valley fill A3 (Be1 and Be5; Fig. 2) or during the subsequent postglacial incision (Be7; Fig. 2). These data have been previously reported by Brocard et al. (2003), who used NIST normalization for calculating ^{10}Be concentrations and a Sea-Level High-Latitude (SLHL) production rate for ^{10}Be of 5.75 at. g^{-1} yr^{-1} (Dunai, 2000). We have recalculated the reported ^{10}Be concentrations using the standard 07KNSTD normalization (see Table S1 for details). The SLHL ^{10}Be production rate was re-evaluated using the CREp program (Martin et al., 2017; https://crep.otelo.univ-lorraine.fr/#/init). We evaluated an updated SLHL ^{10}Be production rate of 4.11 ± 0.19 at. g^{-1} yr^{-1} using the Lal-Stone scaling scheme (Lal, 1991; Stone, 2000). The ERA-40 reanalysis data set (Uppala et al., 2005) and the atmospheric ^{10}Be-based VDM geomagnetic database (Muscheler et al., 2005) were used to correct atmospheric pressure and geomagnetic field fluctuations, respectively. Corrections for topographic shielding based on field measurements by Brocard et al. (2003) were also applied (Table S1; Dunne et al., 1999).

Brocard et al. (2003) provided sedimentological descriptions of the Drac terraces and collected several depth profiles, which they modelled using a fitting code developed in-house. In order to provide more statistically robust best-fit terrace-abandonment ages from ^{10}Be concentrations along depth profiles, we remodelled the profiles using the Monte-Carlo approach of Hidy et al. (2010). 100 000 simulations were performed for each depth profile, using a soil/sediment density range of 1.7–2.3 g/cm^3 (Brocard et al., 2003), and a maximum terrace erosion rate of 1 cm/yr together with a maximum total erosion of 15 cm. We estimated a range of ^{10}Be inheritance values based on the Be1 depth profile, which has the highest number of data. We used the maximum inheritance value of 3.4 × 10^4 at g^{-1} allowed by this profile as the maximum limit for the other depth profiles (Figs. S1–S3). Finally, after preliminary sensitivity tests and to speed up the Monte-Carlo inversion, we prescribed maximum age constraints of 30, 40 and 20 ka for terraces Be1, Be5 and Be7, respectively (Figs. S1–S3).

4. Results

4.1. 3D reconstruction of (paleo-)Drac profiles

Our 3D-mapping approach allowed us to construct a map of the paleo-valleys and to extract the longitudinal profiles of both the modern Drac and its successive paleo-valleys. The paleo-valley map (Fig. 5A)

Table 1
Sample details and feldspar luminescense (IRSL-50) dating results. Analytical details and measurement protocols are given in the main text.

Sample (*aliquots*)	Location (WGS84)		Elevation (m a.s.l)	Radionuclide concentration			Total dose rate[a] (Gy/ka)	CAM[b] uncorrected De	MAM[c] uncorrected De	OD[b]	Fading[d] (g_{2days})	Corrected age[e] (ka)
	°N	°E		K (%)	Th (ppm)	U (ppm)		(Gy)	(Gy)	(%)	(%/decade)	
D01 (*19*)	44.876	5.6989	528	2.33 ± 0.02	6.34 ± 0.15	1.44 ± 0.31	3.93 ± 0.26	366.7 ± 15.5	/	13.2	3.78 ± 0.54	137 ± 15
D02 (*24*)	44.884	5.7969	622	2.46 ± 0.03	7.59 ± 0.19	1.69 ± 0.18	4.19 ± 0.26	136.8 ± 5.7	/	14.5	3.3 ± 0.5	44 ± 4
D03 (*16*)	44.818	5.9125	767	2.61 ± 0.03	7.30 ± 0.37	1.36 ± 0.37	4.19 ± 0.26	323.5 ± 22.1	258 ± 28.6	24.6	3.75 ± 0.6	90 ± 14
D04 (*8*)	44.87	5.8429	852	1.92 ± 0.02	4.93 ± 0.08	1.21 ± 0.13	3.3 ± 0.16	445.0 ± 30.4	/	17.0	5.06 ± 0.63	234 ± 33
D05 (*6*)	44.962	5.6995	744	1.56 ± 0.02	4.53 ± 0.11	1.28 ± 0.11	3.06 ± 0.24	463.2 ± 20.2	/	6.7	2.9 ± 0.5	203 ± 23
D06 (*22*)	45.008	5.6956	419	1.78 ± 0.02	4.54 ± 0.10	1.06 ± 0.18	3.05 ± 0.16	160.6 ± 8.0	145.7 ± 11.8	20.0	2.42 ± 0.37	60 ± 6
D07 (*21*)	44.946	5.6801	535	2.31 ± 0.02	9.17 ± 0.16	2.26 ± 0.17	4.23 ± 0.17	372.0 ± 18.1	/	17.6	3.19 ± 0.51	121 ± 11
D11 (*22*)	44.793	5.9133	915	0.64 ± 0.02	3.00 ± 0.08	1.49 ± 0.57	2.04 ± 0.17	103.0 ± 17.1	26.5 ± 4.1	76.5	5.23 ± 1.43	21 ± 7
D12 (*27*)	44.785	5.9183	760	0.45 ± 0.01	1.76 ± 0.11	0.87 ± 0.14	1.66 ± 0.24	101.6 ± 16.5	25.7 ± 3.7	83.2	3.93 ± 0.68	22 ± 5
D15 (*21*)	44.812	5.9019	881	0.21 ± 0.00	1.14 ± 0.05	1.11 ± 0.33	1.42 ± 0.15	186.5 ± 15.9	131.4 ± 14.5	36.6	3.36 ± 0.35	130 ± 21
D16 (*16*)	44.812	5.9003	863	0.30 ± 0.01	1.25 ± 0.04	1.19 ± 0.12	1.57 ± 0.14	156.3 ± 23.8	61.2 ± 10.2	59.6	4.16 ± 0.73	58 ± 13

Notes: The coarse-grained fraction of 180–300 μm was isolated for samples D01, D02, D03, D05 and D12, and 180–250 μm for samples D04, D06, D07, D11, D15 and D16. 24 aliquots for each sample were mounted on stainless-steel discs for luminescence measurements, the number of aliquots that provided an individual De (Equivalent Dose, Gy) estimate is reported in left column for each sample (in *italics*).

[a] Dose rate calculations were performed with DRAC (Durcan et al., 2015), assuming water content of 7 ± 3%, an internal K-content of 12.5 ± 0.5% (Huntley and Baril, 1997) and an alpha efficiency value of 0.15 ± 0.05 (Balescu and Lamothe, 1994).

[b] CAM = Central Age Model, OD = overdispersion of De distribution (Galbraith et al., 1999).

[c] MAM = Minimum Age Model (Galbraith and Green, 1990); applied for De distributions with OD > 20%. A sigma-b (σb) value of 0.15 was used based on other samples that show OD values averages ~15%. No MAM was run for samples with OD <20%.

[d] Final fading-corrected ages were calculated following the fading correction procedure of Huntley and Lamothe (2001), with g_{2days} values measured for 3 aliquots per sample.

[e] For all the samples except D03, D06, D11, D12, D15 and D16, fading-corrected CAM ages are reported. For D03, D06, D11, D12, D15 and D16, the fading-corrected MAM ages are shown.

shows that the thalweg of the Drac river has not shifted laterally by more than 3 km from V1 to V3 and has remained contained within the wider Drac valley. A complete extraction of the river long profile was conducted along the present-day valley and along the V3 paleo-valley, while long profiles of paleo-valleys V2 and V1 could only be partially reconstructed (Figs. 5 and 7).

The geometries of the three paleo-valleys are particularly well constrained along a 20-km long reach of the Drac located around the Monteynard dam (Fig. 2), in the northern part of the study area (Fig. 5). Further upstream, the base of V1 has been completely eroded. Upstream of Monteynard, both the V2 and V3 long profiles have been reconstructed. The profiles of V1, V2 and V3 are not parallel to the modern profile of the Drac river. At the Monteynard dam, both the modern Drac river and the V2 profiles show a knickpoint that is about 40 m high. In contrast, V1 and V3 do not show any knickpoint in this reach. As a consequence, V3 hangs above the present-day profile of the Drac by about 30 m downstream of the Monteynard dam, whereas the base of V3 lies below the modern Drac river under the Monteynard reservoir. From 35 to 60 km upstream of the Romanche confluence, V3 hangs above the modern Drac profile by about 20 m. Further upstream, under the Sautet reservoir, V3 is again incised to below the modern Drac profile. The alluvial fills A1, A2 and A3 also show variable thicknesses of about 140 m, 180 m and 120 m, respectively (Fig. 7).

4.2. Feldspar luminescence dating

Sample-specific information and results of total dose rate, De, fading and age calculations are presented in Table 1. IRSL-50 De results and distributions for all samples, along with CAM and MAM De estimates, are provided in Figs. S4–S5. Large differences in total dose rates and overdispersion are observed between samples. Dose rates for the Drac samples are between 3.0 and 4.2 Gy ka^{-1}, while dose rates for the Souloise samples are between 1.4 and 2.0 Gy ka^{-1}. This difference can be attributed to differences in sediment provenance between the Drac and the Souloise rivers: the Drac river drains the western flank of the Pelvoux massif, which is mainly composed of crystalline rocks rich in radiogenic elements, whereas the Souloise catchment is composed of mainly calcareous sedimentary rocks that are poor in radiogenic elements. A significant difference in bleaching is also observed between the Drac and Souloise samples: OD values for the Drac samples range between 6 and 24%, while OD values for the Souloise samples are between 36 and 83%, suggesting shorter transport distances and lower bleaching efficiency prior to deposition.

Feldspar IRSL-50 ages for samples from the A1 fill are between 203 ± 23 ka (D05) and 234 ± 33 ka (D04); these samples were collected toward the top and middle of the fill, respectively (Fig. 7). IRSL-50 data for A1 sediment fills show apparent saturation in most analysed aliquots (Table 1, Fig. S4); thus, the inferred burial ages of these samples should be considered as minimum estimates. Moreover, 200–250 ka is close to the age-range limit for feldspar IRSL-50 dating (Buylaert et al., 2012). A2 ages all overlap, and range between 121 ± 11 ka (D07) and 137 ± 15 ka (D01), suggesting rapid sediment aggradation (Fig. 7). In the downstream reach of A2, IRSL-50 data show efficient bleaching in samples D01 and D07 (Figs. S4–S5), while in the upper reaches of the Drac (D15) the OD value is much higher (Table 1, Fig. S5), suggesting proximal sediment deposition. Finally, IRSL-50 results from the paleo-Drac fill A3

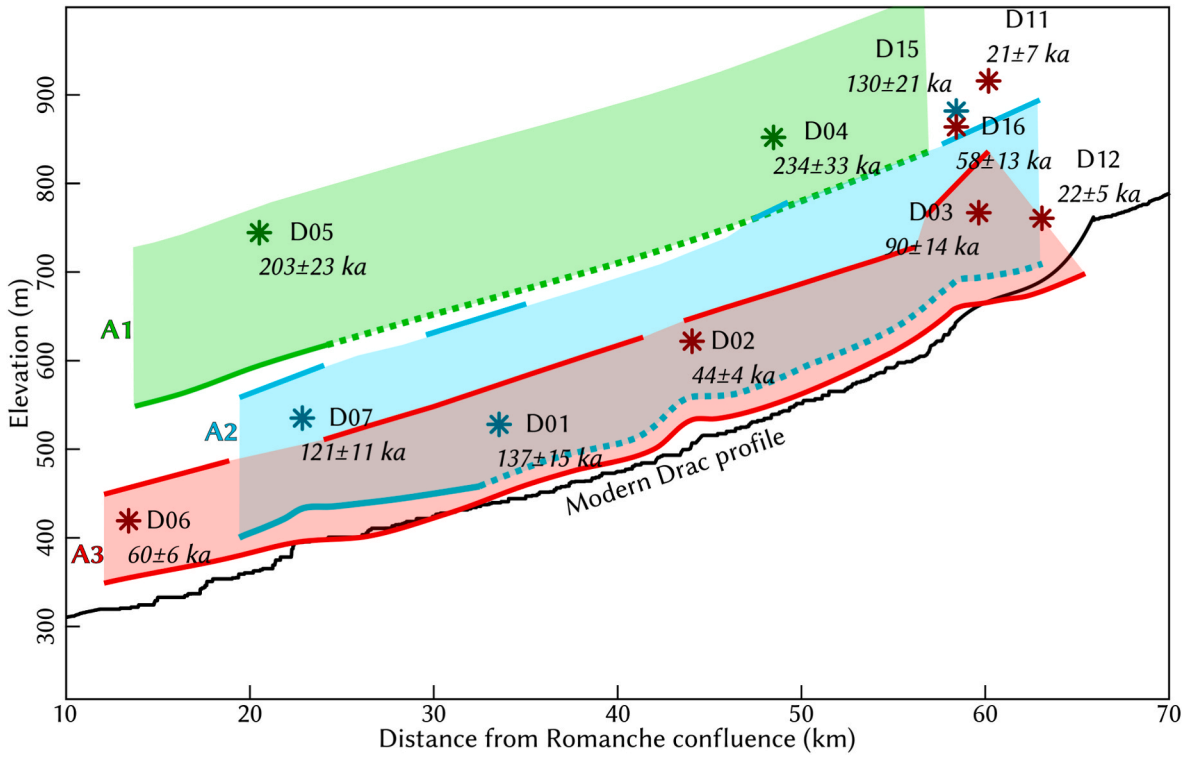

Fig. 7. Reconstruction of the Drac paleo-valleys in the studied area. Green, blue and red colors represent paleo-valley fills A1, A2 and A3, respectively. Solid line contours indicate that the base or top of the paleo-valley fills are constrained by mapped outcrops. Only the geometry of the most recent paleo-valley fill A3 is constrained along the entire course of the Drac. Feldspar luminescence dating results are plotted on the profile (colored stars, age in italics). Note the staggering of the three paleo-valley profiles and the difference in fill thickness between A2 and A3.

strongly suggest poly-phased sediment aggradation (Fig. 7). The oldest ages of 90 ± 13 ka (D03) and 58 ± 13 ka, (D16) suggests early, protracted alluvial deposition in the upstream reaches of the Drac River; in contrast, the downstream reaches record younger ages between 44 ± 4 ka (D02) and 60 ± 6 ka (D06). Finally, the upper reaches of the Drac (samples D11 and D12, Fig. 7) also highlight a rapid second period of alluvial deposition between 22 ± 5 and 21 ± 7 ka.

4.3. Recalculated ^{10}Be exposure ages of Drac terraces

Recalculated ^{10}Be concentrations for the Drac fluvial terraces Be1, Be5 and Be7 (see Fig. 2 for locations) are provided in Table S1. Using the updated ^{10}Be production rate and Monte-Carlo concentration-depth profile simulations (Hidy et al., 2010), we re-evaluated the terrace abandonment ages along the Drac profile. Upper fluvial terraces reveal asynchronous abandonment along the Drac (Figs. S1–S2), with a relatively young exposure age for Be1, sampled just upstream of the

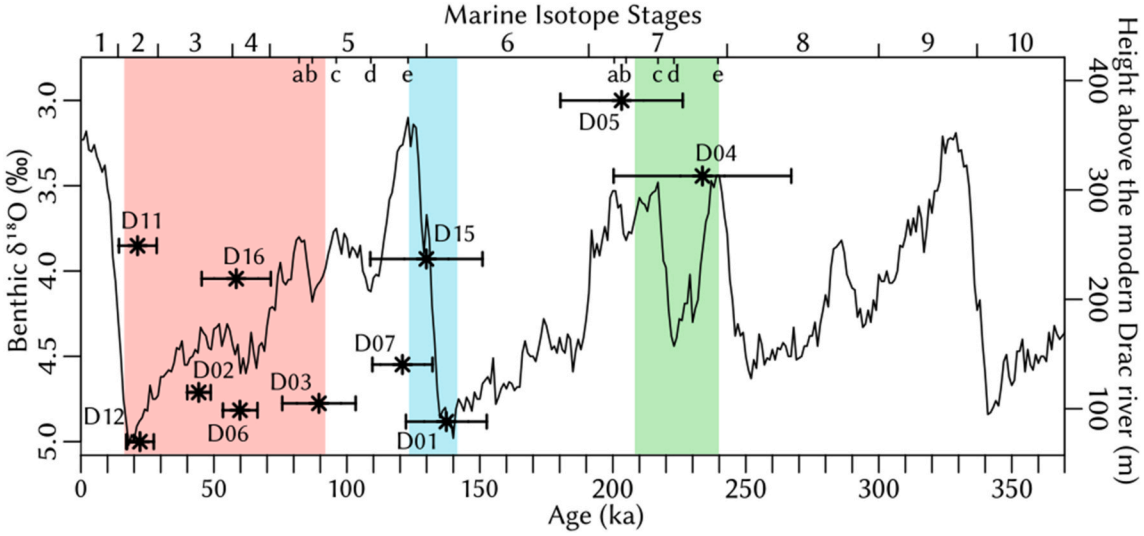

Fig. 8. Luminescence-dating constraints for alluvial fills of the paleo-valleys V1 (A1 - green), V2 (A2 - blue) and V3 (A3 - red) correlated to the Middle-Late Pleistocene climatic cycles recorded by the benthic $\delta^{18}O$ stack (left axis, Lisiecki and Raymo, 2005) and Marine Isotope Stages (MIS, top axis). Luminescence samples are reported based on their elevation relative to the modern Drac riverbed (right axis).

Monteynard reservoir (range: 11.4–17.1 ka, mode: 13.9 ka, best-fit model: 13.5 ka, Fig. S1), and an older exposure age for Be5, collected upstream of the confluence of the Drac and Souloise Rivers (range: 17.8–35.2 ka, mode: 22.8 ka, best-fit model: 27.2 ka, Fig. S2). A lower strath terrace adjacent to the Monteynard reservoir (Be7) provides a younger exposure age from our depth-profile modelling approach (range: 9.5–15.2 ka, mode: 11.7 ka, best-fit model: 12.5 ka, Fig. S3), which is consistent with the position of Be7 close to the modern Drac profile and with the chronology provided by Brocard et al. (2003).

5. Discussion

Fig. 8 shows a tentative correlation between the burial ages for the Drac alluvial sediment fills A1, A2 and A3, and the Middle-Late Pleistocene global climatic evolution. Our dating results show several phases of alluviation along the Drac profile between ca. 20 and ca. 230 ka. Paleo-valley V1 was filled (fill A1) during MIS 7, and considering both the minimum-age estimates for samples D04 and D05 and the overlapping error bars, alluviation probably occurred around 210–230 ka, covering one or several sub-stages: MIS 7b-c and/or d. Based on the global paleoclimatic record, we favour the cold stage MIS 7d as the most probable time of alluviation (Fig. 8). Alluvial deposition of fill A2 (samples D01, D07 and D15, Fig. 7) occurred during the late MIS 6 to early MIS 5, around ~120–140 ka (Fig. 8). Our luminescence ages for fill A3 show a more complex geomorphic and depositional history: the variable ages for A3 (samples D02, D03, D06, D11, D12, and D16, Fig. 7) imply that alluvial filling occurred during several phases spanning MIS 2-MIS 4, and possibly extending to MIS 5b; i.e., between ca. 20 ka and ca. 90 ka (Fig. 8).

5.1. Early, pleni and late-glacial aggradation dynamics of the Drac

Feldspar IRSL-50 dates of alluvial fills A1, A2 and A3 show a reasonable first-order correlation between phases of sediment aggradation and the cold periods MIS 7d, MIS 6, and MIS 4 to MIS 2, respectively (Fig. 8). However, the chronology of alluviation appears to differ significantly between A3 and A2. Burial ages for A3 are spread over more than 60 ka between the end of MIS 5 and MIS 2, which suggests poly-phased filling of the V3 paleo-valley. In contrast, the burial ages for the alluvial fill A2 are centred on the glacial-interglacial transition between late MIS 6 and early MIS 5, suggesting rapid, single-phased sediment aggradation during late-glacial times. The available IRSL-50 dates for the A1 fill, although associated with larger uncertainties, are potentially consistent with similar sediment aggradation dynamics as for A2; i.e., rapid deposition at the MIS 7c-d transition (Fig. 8).

Morpho-sedimentary observations also suggest a difference in alluvial dynamics between A2 and A3, which is most clearly evidenced in the downstream reaches of the Drac River at Monteynard dam (Fig. 3). The sedimentary matrix of sample D07 (fill A2) is poorly sorted and rich in clay, unlike samples D02 and D06 (fill A3) that rather have a sandy matrix. This difference suggests fluvio-glacial sedimentation and proximity to the upstream glacier(s) when fill A2 was deposited. In addition, the filling sequence is different between fills A2 and A3 (Fig. 3). Fill A2 is composed of a 170-m thick monotonic coarse-clastic sequence, whereas the A3 fill sequence is around 210 m thick; 120 m of fluvial sediments (where we collected the luminescence samples) at the base are covered by 90 m of glacio-lacustrine clays and a further 200 m of glacial till. Between the fluvial sediments and the clay sequence, a sandy interval of few meters thick marks the transgression of the Trièves lake on the fluvial sediments composing the base of A3. In contrast, the 170-m thick coarse A2 fill is topped by an indurated abandonment surface showing ripple marks, and does not record a Trièves paleo-lake transgression (Brocard, 2002). These geochronological and morpho-sedimentary arguments suggest that the climatic and glacial configurations of the downstream Drac area were different at the times of deposition of the A2 and A3 fills. We thus propose that the A2 fill sequence was deposited during a late-glacial phase (i.e., late MIS 6 to early MIS 5; Fig. 8) associated with the onset of climate warming and ice retreat. The early retreat of the Drac glacier and the relative persistence of the Isère and Bonne glacier dams, due to different cachment hypsometries and possible transfluence of the Romanche glacier to the Bonne glacier (Fig. 1; Monjuvent, 1978), would have created glacio-lacustrine conditions, and this accommodation space was filled by a significant paraglacial sediment flow in an outwash-plain environment. This interpretation is in agreement with previously proposed paleo-glacial reconstructions implying that the Drac valley was fully glaciated during the MIS 6 glacial maximum (Monjuvent, 1973, 1978). The A2 alluvial sequence would thus have filled a glacially-scoured valley. In contrast, basal fluvial sediments of the A3 fill were probably deposited in a context of early-glacial cooling (e.g., Cordier et al., 2006; Vandenberghe, 2008; Delmas et al., 2015), possibly due to an increasing and coarsening sedimentary input during glacier advance. The clay-rich glacio-lacustrine deposits of the Trieves paleo-lake, making up the top part of the A3 fill, correspond to a pleni-glacial context, during which the Drac River was dammed by the Isère-Romanche glacier (Bièvre and Crouzet, 2021). Finally, the glacial till covering the A3 sequence can be attributed to the LGM period (i.e., MIS 2), when the Isère-Romanche glacier extended furthest into the Drac valley (Fig. 1).

5.2. Downstream Drac fluvial dynamics driven by Isère-Romanche glacier fluctuations

The synthesis of field investigations, 3D mapping, feldspar IRSL-50 dating, bulk-clay ^{14}C dating of lacustrine deposits (Bièvre and Crouzet, 2021), and recalculated ^{10}Be exposure ages of alluvial terraces (Be1, and Be7; Brocard et al., 2003) allows us to propose a detailed temporal model of incision and aggradation dynamics along the Drac river. Following incision of the alluvial valley V2, the downstream Drac valley (Fig. 9A) records a single aggradation/incision cycle during the last ca. 100 ka (not considering potential post-LGM aggradation phases; Brocard, 2002). Initial fluvial aggradation in paleo-valley V3 during the late MIS 4 is relatively slow (~1 mm/yr on average), as constrained by the 60 ± 6 ka age of sample D06 (Fig. 9A). From around 40–50 ka (i.e. early/middle MIS 3), local sedimentation switches to lacustrine conditions and accelerates significantly (~10 mm/yr), as indicated by ^{14}C dating of the Trièves paleo-lake deposits (Bièvre and Crouzet, 2021). This fluvial/lacustrine transition at around 40–50 ka probably marks the onset of downstream ice damming by the Isère-Romanche glacier, consistent with glacier advances in the French western Alps during that period (Gribenski et al., 2021). Glacio-lacustrine sedimentation continued until at least 30 ka, according to the ^{14}C dating. The northern part of the Trièves lake deposits was overridden by the Isère-Romanche glacier during the LGM, as indicated by glacial tills partially overlying these glacio-lacustrine sediments (Figs. 3 and 9A). Maximum glacio-lacustrine aggradation and glacial till deposition can be proposed between ca. 30 and 17 ka if we favour the maximum age estimate for abandonment of the high alluvial terrace from the ^{10}Be profile Be1 (cf. Section 4.3). The extrapolated profile of the high alluvial terrace Be1 suggests a local fluvial base level beneath the glacio-lacustrine clays, showing the progressive flushing of the Trièves lake and a first incision phase driven by base-level drop following thinning of the Isère-Romanche glacier. Deposition of this alluvial strath terrace could mark a phase of relative base-level stability and therefore stable ice thickness of the Isère-Romanche glacier system around 17 ka. After ca. 17 ka, the final retreat of the Isère-Romanche glacier would have caused very rapid incision of the Drac river: up to 300 m in 1–7 ka (in agreement with rates reported in Brocard et al., 2003, Fig. 9A). ^{10}Be exposure dating of glacially polished bedrock in the downstream reach of the Romanche glacier (Séchilienne area, cf. Fig. 1 for location) implies the persistence of the Romanche glacier at an elevation of about 1000 m until ca. 17 ka (Schwartz et al., 2017), which is in excellent agreement

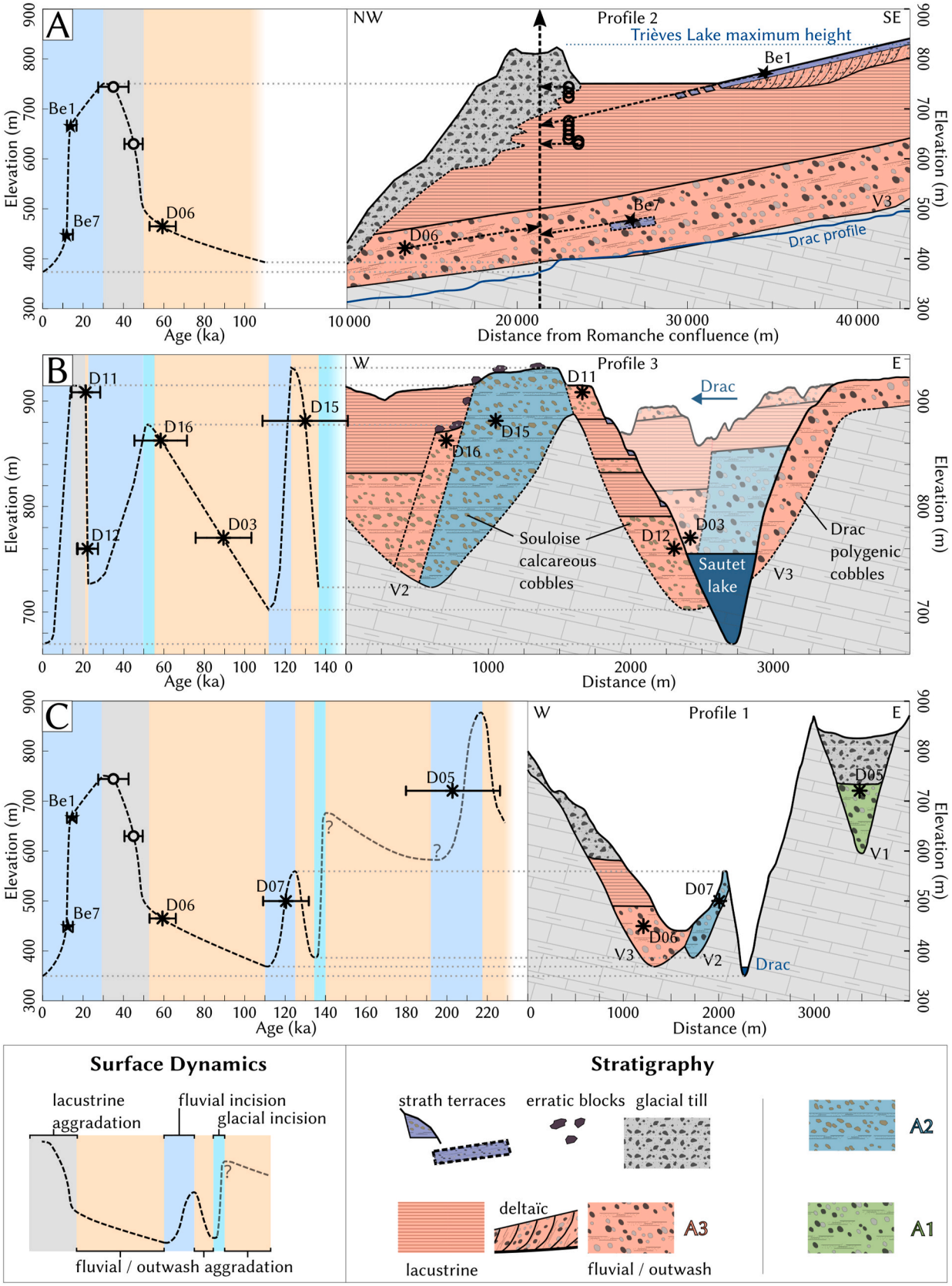

(caption on next page)

Fig. 9. Incision/aggradation models for the Drac paleo-valleys. The right-side panels are geological cross-sections of the paleo-valleys (see Fig. 5A for locations). The curves of the left-side panels show the temporal evolution of the elevation of the Drac riverbed for each profile. The curves are interpreted from geochronological data (see Fig. 2 for locations) and the geometry of the paleo-valley fills. Solid line are observed contacts, dotted lines are inferred contacts **A.** Cross-section of the alluvial fill A3 along the 30-km reach of the Drac immediately upstream of the Drac/Romanche confluence. The synthesis of luminescence, ^{14}C and ^{10}Be dating constraints (see text for discussion) allows a precise reconstruction of the aggradation/incision cycle during the last glacial cycle (since ca. 100 ka). **B.** Cross-section at the Drac-Souloise junction (Sautet reservoir; Profile 3 in Fig. 5A). Semi-transparent profile in the background corresponds to a cross-section of the eastern flank of the Drac valley. Minimum elevations of paleo-valleys V2 and V3 lie above the modern Drac riverbed. Paleo-valley V2 is filled with calcareous gravels brought in by the Souloise River, while paleo-valley V3 is filled with sediments derived from both the Souloise and Drac catchments. Three major cycles of incision/aggradation are highlighted over the last 140 ka. **C.** Cross-section at the Monteynard dam (Profile 1 in Fig. 5A) and reconstruction of the incision/aggradation phases since 220 ka with the three generations of the Drac paleo-valleys.

with our maximum abandonment age estimate for the Be1 fluvial terrace and with our local model of fluvial dynamics (Fig. 9A). Rapid fluvial incision after ca. 17 ka for the downstream reach of the Drac would thus be linked to a rapid base-level drop following ice retreat. This rapid glacier retreat left a large pro-glacial lake in the present-day Isère valley upstream of its confluence with the Romanche (Fig. 1), which filled up with lacustrine and fluvial sediments over several thousand years during the Late-glacial period (Monjuvent, 1978; Nicoud et al., 2002). The above model of glacio-fluvial dynamics for the downstream Drac reach has a high spatio-temporal resolution, obtained by integrating independent geochronological data, and reflects the strong sensitivity of the dynamics of the Drac fluvial system to spatio-temporal fluctuations in the Isère-Romanche glacier system.

5.3. *Upstream fluvial dynamics controlled by fluctuations of the Drac and Bonne glaciers*

The aggradation/incision model inferred from geochronological and morpho-sedimentary data in the upstream Drac reaches (Fig. 9B) differs from that for the downstream reaches. The upstream Drac, around the Drac-Souloise confluence and the modern Sautet dam, is characterized by a complex interlocking of alluvial terraces containing fluvial material transported by both the Drac (characterised by cobbles with multiple sedimentary and crystalline lithologies) and the Souloise (dominated by limestone cobbles) rivers. Three aggradation/incision cycles can be inferred since the late MIS 6. At the MIS 6-MIS 5 transition (ca. 130 ka), the higher alluvial fill (A2) was deposited, as constrained by luminescence dating results (sample D15, Figs. 7 and 9B), followed by incision during MIS 5. A second aggradation phase (with aggradation rates of ~0.3 cm/yr) occurred during the cooling period marking the end of MIS 5 to the early MIS 4, constrained by the ages of samples D03 and D16 (Figs. 7 and 9B). A major advance of the Drac glacier, overriding the alluvial deposits of both the A2 and first A3 fills during the MIS 4 glacial maximum, is attested by field observations of erratic boulders covering these deposits (Fig. 9B; Monjuvent, 1978). This glacial advance stopped aggradation and slightly eroded the alluvial sediments underneath. An incision phase during MIS 3, followed by rapid and significant aggradation (at rates >4 cm/yr) during MIS 2, is required by our chronological constraints of the A3 fill (samples D11 and D12, occurring at similar elevations to samples D16 and D03, respectively; Fig. 9B). The top of this A3 fill (sample D11; 21 ± 7 ka) corresponds to the LGM (in agreement with the abandonment age of this fill surface of $22.8^{+12.4}_{-5.0}$ ka modelled from the cosmogenic profile Be5; Fig. S2), after which rapid incision shaped the present-day Drac and Souloise valleys.

This paleo-glacial and paleo-environmental reconstruction highlights a dual glacial control on the aggradation/incision history of the upstream Drac valley (Fig. 1). Fluctuations of the Bonne glacier control the base level of this part of the drainage system by periodically blocking the Drac valley. Upstream, the Drac glacier controls alluviation by supplying variable amounts of water and sediment, but can also advance downstream and thus erode previously deposited sediments. Similar aggradation processes are observed for the downstream Drac reaches: late-glacial alluviation followed the rapid retreat of the Drac glacier at the MIS 6-MIS 5 transition, leading to the A2 alluvial fill (sample D07; Fig. 9C). Alluviation during the late MIS 5-MIS 4 may be poly-phased and appears to be relatively slow, in both the upstream and downstream Drac reaches (Fig. 9B and Fig. 9C). In contrast, very rapid alluviation during MIS 2 is most likely due to the rapid advance of the Isère-Romanche glacier for the downstream reach of the Drac, and to the Bonne glacier combined with high sediment delivery at the Souloise-Drac junction for the upstream reach.

The geomorphic aggradation/incision models shown in Fig. 9 highlight the strong coupling between the fluvio-glacial dynamics of the Drac and both upstream and downstream glacier oscillations. These models therefore have implications for local glacial dynamics. Our paleo-glacier reconstructions are consistent with a fully glaciated Drac valley during the MIS 6 glacial maximum, as described in the literature (Monjuvent, 1973, 1978). Furthermore, and as indicated by observed erratic boulders overlying both the A2 fill and the lower part of the A3 fill at the Drac-Souloise confluence (Fig. 9B; Section 5.3), the Drac paleo-glacier advanced further during MIS 4 than during MIS 2, when it remained confined to the upstream part of the study area (Fig. 1). A comparison of the fluvio-glacial dynamics of the Drac between the upstream zone, where the base level was controlled by the Bonne glacier, and the downstream zone, where the base level was controlled by the Isère-Romanche glacier, suggests that the Bonne glacier was more sensitive to climatic oscillations than the Isère-Romanche system: the downstream Drac reach evidences slow and progressive sediment aggradation during MIS 4, an increase in sediment deposition rate and no apparent incision phase during MIS 3 and a further increase in sediment deposition rate during MIS 2 (Fig. 9A). In contrast, the upstream Drac reach shows more rapid sediment aggradation during MIS 4 and an incision phase during MIS 3 before very rapid sediment deposition during MIS 2 (Fig. 9B). Such differences in paleo-glacier dynamics may be expected because the Isère-Romanche glacier system is much larger than the Bonne glacier and would thus react more sluggishly to rapid climatic variations, as also suggested for other glacier systems in the Alps (e.g., Monegato et al., 2017; Braakhekke et al., 2020).

5.4. *Long-term incision dynamics of the Drac valley*

Our geochronological and morpho-sedimentary data also have important implications to understand the long-term incision dynamics of the Drac River. Our study confirms that incision of the Drac during the Late and Middle Pleistocene was multi-phased, and strongly controlled by climatic oscillations and glacial fluctuations. At least four epigenetic fluvial incision phases were triggered by the warmer climatic stages (MIS1, 3, 5 and 7; Fig. 9).

A glacial incision phase affecting the entire Drac valley occurred during the MIS 6 glacial maximum. Our data do not allow quantifying the respective contribution of post-A1 fluvial incision (i.e., during MIS 7a-c; see below for discussion) and of glacial erosion during MIS 6. Nonetheless, the significant difference in elevation between the paleo-valley bases V1 and V2, and the scarcity of sediment sequences predating MIS 6 (the only remnants in our study area being the A1 fill sediments attributed to MIS 7d), suggest that the MIS-6 Drac glacier eroded most of the older alluvial sediments and significantly carved the V2 paleo-valley.

The area around the Monteynard dam (Figs. 3 and 9C) provides an opportunity to quantify the long-term incision of the Drac because at

least three epigenetic gorges (V1, V2 and V3, Fig. 3) and associated alluvial fill sequences (A1, A2 and A3) are preserved. Both the formation and preservation of these narrow epigenetic gorges at this location can be attributed to the locally very resistant bedrock lithology, consisting of thick-bedded Liassic limestones. The late-Pleistocene incision history is well constrained for V2 (MIS 6), V3 (MIS 5) and for the modern Drac valley, allowing us to calculate an incision rate of 0.2–0.3 mm/yr over the last 120–140 ka. The earlier incision history is more fragmentary (Fig. 9C). Given our current data, we cannot conclude whether fill A1 is of pre-glacial or late-glacial origin. Similarly, whether the V1 paleo-valley was formed by glacial or fluvial incision remains unconstrained. We cannot therefore give an absolute age for the V1 paleo-valley. However, we have established that the epigenetic cycles of the Drac valley have been linked to the late-Pleistocene climatic oscillations and can be temporally correlated to the Marine Isotope Stages (Lisiecki and Raymo, 2005), with estimated age constraints for the A1 fill of ca. 220–240 ka (Fig. 7). We thus have sufficient constraints to confidently give an age interval for the V1 paleo-valley of around 240 ka (i.e., MIS 7e) or older (possibly up to MIS 9, as suggested by our maximum age estimate of A1; Fig. 8). This age interval implies average incision rates estimate between 0.6 and 0.8 mm/yr over the Mid-to Late-Pleistocene times and between 0.8 and 1.6 mm/yr from V1 to V2. These estimates suggest a possible slowdown in the long-term incision of the Drac valley since the end of MIS 6. We interpret this decrease in valley incision rate as reflecting the signature of strong MIS 6 glacial incision along the Drac valley.

Brocard et al. (2003) calculated an incision rate of 0.8 mm/yr over the last 190 kyr for the Buëch valley, located around 40 km south of our study area, from alluvial-terrace dating. Our long-term incision-rate estimates (0.6–0.8 mm/yr from V1) show good agreement with the estimates from the Buëch, as well as with more recent rock-uplift data from levelling and GPS measurements for the Western Alps (Nocquet et al., 2016). This may suggest that isostatic uplift can be considered as the main driver for our long-term inferred valley incision rates for the Drac river. These rates are, however, significantly higher than late-Pleistocene to Holocene incision rates derived from fluvial bedrock gorges in the Southwestern Alps of around 0.2 mm/yr (Petit et al., 2017; Cardinal et al., 2022).

6. Conclusions

We have combined a synthesis of new and published geochronological data with 3D mapping of the Quaternary sedimentary archives (specifically alluvial deposits) along the Drac valley, with the aim of highlighting the close spatial and temporal coupling between glacier dynamics, alluvial to glacio-lacustrine sedimentation and valley incision. Our results show that the dynamics of the Drac valley are highly sensitive to Pleistocene climatic variations and boundary conditions from the surrounding main valleys. The evolution of the valley is asymmetrical, with phases of rapid incision at the start of interglacials and longer phases of aggradation that are temporally heterogeneous: pleni-glacial and late-glacial aggradation rates are approximately ten times faster than early-glacial aggradation rates. While early-glacial aggradation seems to be widespread and spatially relatively homogeneous, pleni-glacial and late-glacial aggradation is spatially heterogeneous and asynchronous due to its control by local glacial dynamics. In addition, our incision/aggradation models allow us to better constrain the dynamics of the surrounding main glaciers: the major Isère-Romanche glacier system appears to have reacted to climatic variations with more inertia than local glaciers, such as the Bonne or Drac, revealing potential specificities in catchment hypsometry or/and precipitation during glacial stages. Finally, we constrained a mean long-term incision rate of 0.6–0.8 mm/yr for the Drac valley over the last ca. 250 ka, which is not constant but rather seems to depend on the magnitude of local glaciations, once again demonstrating the complex geomorphic response of the Drac drainage system that is highly sensitive to Pleistocene paleo-climatic and paleo-environmental conditions.

CRediT authorship contribution statement

Vivien Mai Yung Sen: Conceptualization, Formal analysis, Investigation, Methodology, Visualization, Writing – original draft. **Pierre G. Valla:** Conceptualization, Formal analysis, Funding acquisition, Investigation, Methodology, Supervision, Visualization, Writing – review & editing. **Peter A. van der Beek:** Conceptualization, Funding acquisition, Investigation, Methodology, Supervision, Visualization, Writing – review & editing. **François Lemot:** Conceptualization, Formal analysis, Investigation, Methodology, Visualization, Writing – review & editing. **Christian Crouzet:** Conceptualization, Methodology, Visualization, Writing – review & editing. **Gilles Brocard:** Conceptualization, Methodology, Visualization, Writing – review & editing.

Declaration of competing interest

The authors declare that they have no known competing financial interests or personal relationships that could have appeared to influence the work reported in this paper.

Data availability

Data will be made available on request.

Acknowledgments

The authors warmly thank C. Ariagno, A. de Leeuw and T. Schildgen for their help during fieldwork. N. Gribenski and E. Serra are thanked for help with luminescence analyses at the University of Bern. This study was supported by the French ANR-PIA programme (ANR-18-MPGA-0006). We thank two anonymous reviewers for constructive comments on an earlier version of this manuscript, and Prof. Colm O'Cofaigh for efficient editorial handling.

Appendix A. Supplementary data

Supplementary data to this article can be found online at https://doi.org/10.1016/j.quascirev.2024.108632.

References

Anselmetti, F.S., Bavec, M., Crouzet, C., Fiebig, M., Gabriel, G., Preusser, F., Ravazzi, C., DOVE scientific team, 2022. Drilling Overdeepened Alpine Valleys (ICDP-DOVE): quantifying the age, extent, and environmental impact of Alpine glaciations. Sci. Drill. 31, 51–70. https://doi.org/10.5194/sd-31-51-2022.

Aitken, M.J., 1985. Thermoluminescence dating: past progress and future trends. Nucl. Tracks Radiat. Meas. 10, 3–6. https://doi.org/10.1016/0735-245X(85)90003-1.

Auclair, M., Lamothe, M., Huot, S., 2003. Measurement of anomalous fading for feldspar IRSL using SAR. Radiat. Meas. 37, 487–492. https://doi.org/10.1016/S1350-4487(03)00018-0.

Balescu, S., Lamothe, M., 1994. Comparison of TL and IRSL age estimates of feldspar coarse grains from waterlain sediments. Quat. Sci. Rev. 13, 437–444.

Bièvre, G., Crouzet, C., 2021. Multi-proxy analysis of boreholes in remolded Quaternary paraglacial deposits (Avignonet landslide, French Western Alps). Eng. Geol. 286, 106073 https://doi.org/10.1016/j.enggeo.2021.106073.

Braakhekke, J., Ivy-Ochs, S., Monegato, G., Gianotti, F., Martin, S., Casale, S., Christl, M., 2020. Timing and flow pattern of the Orta glacier (European Alps) during the last glacial maximum. Boreas 49, 315–332. https://doi.org/10.1111/bor.12427.

Bridgland, D., Westaway, R., 2008. Climatically controlled river terrace staircases: a worldwide Quaternary phenomenon. Geomorphology 98, 285–315. https://doi.org/10.1016/j.geomorph.2006.12.032.

Brocard, G., 2002. Origine, variabilité spatio-temporelle et signature morphologique de l'incision fluviatile dans les Alpes dauphinoises (SE France). Université Joseph Fourier, Grenoble, Géologie Alpine, Mém. H.S. 43, 168. PhD Thesis.

Brocard, G.Y., van der Beek, P.A., Bourlès, D.L., Siame, L.L., Mugnier, J.-L., 2003. Long-term fluvial incision rates and postglacial river relaxation time in the French Western Alps from ^{10}Be dating of alluvial terraces with assessment of inheritance, soil development and wind ablation effects. Earth Planet Sci. Lett. 209, 197–214. https://doi.org/10.1016/S0012-821X(03)00031-1.

Bull, W.B., 1991. Geomorphic Responses to Climatic Change. Oxford University Press, Oxford, p. 326.

Buylaert, J.-P., Jain, M., Murray, A.S., Thomsen, K.J., Thiel, C., Sohbati, R., 2012. A robust feldspar luminescence dating method for Middle and Late Pleistocene sediments. Boreas 41, 435-451. https://doi.org/10.1111/j.1502-3885.2012.00248.x.

Cardinal, T., Petit, C., Rolland, Y., Audin, L., Schwartz, S., Valla, P.G., Zerathe, S., Régis, B., Aster Team, 2022. Fluvial bedrock gorges as markers for Late-Quaternary tectonic and climatic forcing in the Southwestern Alps. Geomorphology 418, 108476. https://doi.org/10.1016/j.geomorph.2022.108476.

Champagnac, J.D., Molnar, P., Anderson, R.S., Sue, C., Delacou, B., 2007. Quaternary erosion-induced isostatic rebound in the western Alps. Geology 35, 195–198. https://doi.org/10.1130/g23053a.1.

Champagnac, J.-D., van der Beek, P., Diraison, G., Dauphin, S., 2008. Flexural isostatic response of the Alps to increased Quaternary erosion recorded by foreland basin remnants, SE France. Terra. Nova 20, 213–220. https://doi.org/10.1111/j.1365-3121.2008.00809.x.

Clark, P.U., Dyke, A.S., Shakun, J.D., Carlson, A.E., Clark, J., Wohlfarth, B., Mitrovica, J. X., Hostetler, S.W., McCabe, A.M., 2009. The last glacial maximum. Science 325, 710–714. https://doi.org/10.1126/science.1172873.

Colarossi, D., Duller, G.A.T., Roberts, H.M., Tooth, S., Lyons, R., 2015. Comparison of paired quartz OSL and feldspar post-IR IRSL dose distributions in poorly bleached fluvial sediments from South Africa. Quat. Geochronol. 30, 233–238. https://doi.org/10.1016/j.quageo.2015.02.015.

Cordier, S., Harmand, D., Frechen, M., Beiner, M., 2006. Fluvial system response to middle and upper Pleistocene climate change in the Meurthe and Moselle valleys (eastern Paris basin and Rhenish massif). Quat. Sci. Rev. 25, 1460–1474. https://doi.org/10.1016/j.quascirev.2005.11.007.

Cordier, S., Adamson, K., Delmas, M., Calvet, M., Harmand, D., 2017. Of ice and water: Quaternary fluvial response to glacial forcing. Quat. Sci. Rev. 166, 57–73. https://doi.org/10.1016/j.quascirev.2017.02.006.

Coutterand, S., 2010. Etude géomorphologique des flux glaciaires dans les Alpes nord-occidentales au Pléistocène récent. Université de Savoie, Chambéry, France, p. 471. PhD Thesis.

Dehnert, A., Lowick, S.E., Preusser, F., Anselmetti, F.S., Drescher-Schneider, R., Graf, H. R., Heller, F., Horstmeyer, H., Kemna, H.A., Nowaczyk, N.R., Züger, A., Furrer, H., 2012. Evolution of an overdeepened trough in the northern Alpine foreland at Niederweningen, Switzerland. Quat. Sci. Rev. 34, 127–145. https://doi.org/10.1016/j.quascirev.2011.12.015.

Delmas, M., Braucher, R., Gunnell, Y., Guillou, V., Calvet, M., Bourlès, D., Aster Team, 2015. Constraints on Pleistocene glaciofluvial terrace age and related soil chronosequence features from vertical ^{10}Be profiles in the Ariège River catchment (Pyrenees, France). Global Planet. Change 132, 39–53. https://doi.org/10.1016/j.gloplacha.2015.06.011.

Dieleman, C., Christl, M., Vockenhuber, C., Gautschi, P., Graf, H.R., Akçar, N., 2022. Age of the most extensive glaciation in the Alps. Geosciences 12, 39. https://doi.org/10.3390/geosciences12010039.

Duller, G.A.T., 2015. The Analyst software package for luminescence data: overview and recent improvements. Ancient TL 33, 35–42.

Dunai, T.J., 2000. Scaling factors for production rates of in situ produced cosmogenic nuclides: a critical reevaluation. Earth Planet Sci. Lett. 176, 157–169.

Dunne, J., Elmore, D., Muzikar, P., 1999. Scaling factors for the rates of production of cosmogenic nuclides for geometric shielding and attenuation at depth on sloped surfaces. Geomorphology 27, 3–11.

Durcan, J.A., King, G.E., Duller, G.A.T., 2015. DRAC: dose rate and age calculator for trapped charge dating. Quat. Geochronol. 28, 54–61. https://doi.org/10.1016/j.quageo.2015.03.012.

Ehlers, J., Gibbard, P.L., 2004. Quaternary glaciations – extent and chronology: Part I: Europe. Dev. Quat. Sci. 2, 475. Elsevier, Boston.

Fuchs, M., Owen, L.A., 2008. Luminescence dating of glacial and associated sediments: review, recommendations and future directions. Boreas 37, 636–659. https://doi.org/10.1111/j.1502-3885.2008.00052.x.

Galbraith, R.F., Roberts, R.G., Laslett, G.M., Yoshida, H., Olley, J.M., 1999. Optical dating of single and multiple grains of quartz from Jinmium rock shelter, northern Australia: Part I, experimental design and statistical models. Archaeometry 41, 339–364.

Galbraith, R.F., Green, P.F., 1990. Estimating the component ages in a finite mixture. Int. J. Rad. Appl. and Instr. D. Nucl. Tracks Rad. Meas. 17, 197–206. https://doi.org/10.1016/1359-0189(90)90035-V.

Galbraith, R.F., Roberts, R.G., 2012. Statistical aspects of equivalent dose and error calculation and display in OSL dating: an overview and some recommendations. Quat. Geochronol. 11, 1–27. https://doi.org/10.1016/j.quageo.2012.04.020.

Gegg, L., Anselmetti, F.S., Deplazes, G., Knipping, M., Madritsch, H., Mueller, D., Preusser, F., Vogel, H., Buechi, M.W., 2023. Rinikerfeld Palaeolake (Northern Switzerland) – a sedimentary archive of landscape and climate change during the penultimate glacial cycle. J. Quat. Sci. 38, 174–185. https://doi.org/10.1002/jqs.3471.

Gianotti, F., Forno, M.G., Ivy-Ochs, S., Kubik, P.W., 2008. New chronological and stratigraphical data on the Ivrea amphitheatre (Piedmont, NW Italy). Quat. Int. 190, 123–135. https://doi.org/10.1016/j.quaint.2008.03.001.

Gianotti, F., Forno, M.G., Ivy-Ochs, S., Giovanni, M., Cesare, R., 2015. Stratigraphy of the Ivrea morainic amphitheatre (NW Italy). An updated synthesis. Alp. Medit. Quat. 28, 29–58.

Gillespie, A., Molnar, P., 1995. Asynchronous maximum advances of mountain and continental glaciers. Rev. Geophys. 33, 311–364. https://doi.org/10.1029/95RG00995.

Gribenski, N., Valla, P.G., Preusser, F., Roattino, T., Crouzet, C., Buoncristiani, J.-F., 2021. Out-of-phase Late Pleistocene glacial maxima in the Western Alps reflect past changes in North Atlantic atmospheric circulation. Geology 49, 1096–1101. https://doi.org/10.1130/G48688.1.

Haeuselmann, P., Granger, D.E., Jeannin, P.-Y., Lauritzen, S.-E., 2007. Abrupt glacial valley incision at 0.8 Ma dated from cave deposits in Switzerland. Geology 35, 143. https://doi.org/10.1130/G23094A.

Heiri, O., Koinig, K.A., Spötl, C., Barrett, S., Brauer, A., Drescher-Schneider, R., Gaar, D., Ivy-Ochs, S., Kerschner, H., Luetscher, M., Moran, A., Nicolussi, K., Preusser, F., Schmidt, R., Schoeneich, P., Schwörer, C., Sprafke, T., Terhorst, B., Tinner, W., 2014. Palaeoclimate records 60-8 ka in the Austrian and Swiss Alps and their forelands. Quat. Sci. Rev. 106, 186–205. https://doi.org/10.1016/j.quascirev.2014.05.021.

Hidy, A.J., Gosse, J.C., Pederson, J.L., Mattern, J.P., Finkel, R.C., 2010. A geologically constrained Monte Carlo approach to modeling exposure ages from profiles of cosmogenic nuclides: an example from Lees Ferry, Arizona. Geochem. Geophys. Geosyst., 11, Q0AA10. https://doi.org/10.1029/2010gc003084.

Huff, W.D., 1974. Mineralogy and provenance of Pleistocene lake clay in an alpine region. Geol. Soc. Am. Bull. 85, 1455–1460. https://doi.org/10.1130/0016-7606(1974)85<1455:MAPOPL>2.0.CO;2.

Hughes, P.D., Gibbard, P.L., Ehlers, J., 2013. Timing of glaciation during the last glacial cycle: evaluating the concept of a global 'Last Glacial Maximum' (LGM). Earth Sci. Rev. 125, 171–198. https://doi.org/10.1016/j.earscirev.2013.07.003.

Huntley, D.J., Baril, M.R., 1997. The K content of the K-feldspars being measured in optical dating or in thermoluminescence dating. Ancient TL 15, 11–13.

Huntley, D.J., Lamothe, M., 2001. Ubiquity of anomalous fading in K-feldspars and the measurement and correction for it in optical dating. Can. J. Earth Sci. 38, 1093–1106.

Ivy-Ochs, S., Lucchesi, S., Baggio, P., Fioraso, G., Gianotti, F., Monegato, G., Graf, A., Akçar, N., Christl, M., Carraro, F., Forno, M., Schlüchter, C., 2018. New geomorphological and chronological constraints for glacial deposits in the Rivoli-Avigliana end-moraine system and the lower Susa Valley (Western Alps, NW Italy). J. Quat. Sci. 33, 550–562. https://doi.org/10.1002/jqs.3034.

Ivy-Ochs, S., Monegato, G., Reitner, J.M., 2022. Glacial landscapes of the Alps. In: European Glacial Landscapes. Elsevier, pp. 115–121. https://doi.org/10.1016/B978-0-12-823498-3.00045-5.

Kamleitner, S., Ivy-Ochs, S., Monegato, G., Gianotti, F., Akçar, N., Vockenhuber, C., Christl, M., Synal, H.A., 2022. The Ticino-Toce glacier system (Swiss-Italian Alps) in the framework of the alpine last glacial maximum. Quat. Sci. Rev. 279, 107400 https://doi.org/10.1016/j.quascirev.2022.107400.

Knudsen, M.F., Nørgaard, J., Grischott, R., Kober, F., Egholm, D.L., Hansen, T.M., Jansen, J.D., 2020. New cosmogenic nuclide burial-dating model indicates onset of major glaciations in the Alps during Middle Pleistocene Transition. Earth Planet Sci. Lett. 549, 116491 https://doi.org/10.1016/j.epsl.2020.116491.

Kreutzer, S., Schmidt, C., Fuchs, M.C., Dietze, M., Fuchs, M., 2012. Introducing an R package for luminescence dating analysis. Ancient TL 30, 1–8.

Lal, D., 1991. Cosmic ray labeling of erosion surfaces: in situ nuclide production rates and erosion models. Earth Planet Sci. Lett. 104, 424–439. https://doi.org/10.1016/0012-821X(91)90220-C.

Leith, K., Fox, M., Moore, J.R., 2018. Signatures of late Pleistocene fluvial incision in an alpine landscape. Earth Planet Sci. Lett. 483, 13–28. https://doi:10.1016/j.epsl.2017.11.050.

Lisiecki, L., 2010. Links between eccentricity forcing and the 100,000-year glacial cycle. Nat. Geosci. 3, 349–352. https://doi.org/10.1038/ngeo828.

Lisiecki, L.E., Raymo, M.E., 2005. A Pliocene-Pleistocene stack of 57 globally distributed benthic δ ^{18}O records. Paleoceanography 20, PA1003. https://doi.org/10.1029/2004PA001071.

Lory, C., 1860. Description géologique du Dauphiné (Isère, Drôme, Hautes-Alpes), pour servir à l'explication de la carte géologique de cette province. Bull. Soc. stat. sci. nat. arts industr. dép. Isère, Grenoble, 2e sér 7, 748.

Lowick, S.E., Buechi, M.W., Gaar, D., Graf, H.R., Preusser, F., 2015. Luminescence dating of Middle Pleistocene proglacial deposits from northern Switzerland: methodological aspects and stratigraphical conclusions. Boreas 44 (3), 459–482. https://doi.org/10.1111/bor.12114.

Magrani, F., Valla, P.G., Gribenski, N., Serra, E., 2020. Glacial overdeepenings in the Swiss Alps and foreland: spatial distribution and morphometrics. Quat. Sci. Rev. 243, 106483 https://doi.org/10.1016/j.quascirev.2020.106483.

Mandier, P., 1984. Signification dynamique et climatique des formations et terrasses fluviatiles quaternaires dans les Alpes et leur périphérie. Bull. Assoc. fr. étud. quat. 21, 113–118. https://doi.org/10.3406/quate.1984.1497.

Mandier, P., 2003. Reconstitution de l'expansion glaciaire de piedmont des stades A et D des glaciers würmiens du Rhône et de l'Isère : implication et origine de leur disparité. Quaternaire 14, 129–133. https://doi.org/10.3406/quate.2003.1736.

Martin, L.C.P., Blard, P.-H., Balco, G., Lavé, J., Delunel, R., Lifton, N., Laurent, V., 2017. The CREp program and the ICE-D production rate calibration database: a fully parameterizable and updated online tool to compute cosmic-ray exposure ages. Quat. Geochronol. 38, 25–49. https://doi.org/10.1016/J.QUAGEO.2016.11.006.

McNab, F., Schildgen, T.F., Turowski, J.M., Wickert, A.D., 2023. Diverse responses of alluvial rivers to periodic environmental change. Geophys. Res. Lett. 50 https://doi.org/10.1029/2023gl103075.

Monegato, G., Scardia, G., Hajdas, I., Rizzini, F., Piccin, A., 2017. The Alpine LGM in the boreal ice-sheets game. Sci. Rep. 7, 2078. https://doi.org/10.1038/s41598-017-02148-7.

Monjuvent, G., 1973. La transfluence Durance-Isère. Essai de synthèse du Quaternaire du bassin du Drac (Alpes françaises). Geol. Alpine 49, 57–118.

Monjuvent, G., 1978. Le Drac, Morphologie, Stratigraphie et Chronologie Quaternaires d'un Bassin Alpin. CNRS, Grenoble, p. 431.

Murray, A.S., Wintle, A.G., 2000. Luminescence dating of quartz using an improved single-aliquot regenerative-dose protocol. Radiat. Meas. 32, 57–73. https://doi.org/10.1016/S1350-4487(99)00253-X.

Muscheler, R., Beer, J., Kubik, P.W., Synal, H.-A., 2005. Geomagnetic field intensity during the last 60,000 years based on ^{10}Be and ^{36}Cl from the Summit ice cores and ^{14}C. Quat. Sci. Rev. 24, 1849–1860. https://doi.org/10.1016/j.quascirev.2005.01.012.

Muttoni, G., Carcano, C., Garzanti, E., Ghielmi, M., Piccin, A., Pini, R., Rogledi, S., Sciunnach, D., 2003. Onset of major Pleistocene glaciations in the Alps. Geology 31, 989–992. https://doi.org/10.1130/G19445.1.

Nicoud, G., Royer, G., Corbin, J.C., Lemeille, F., Paillet, A., 2002. Creusement et remplissage de la vallée de l'Isère au Quaternaire récent. Apports nouveaux du forage GMB1 (1999) dans la région de Grenoble (France). Geol. Fr. 2002 (4), 39–49.

Nocquet, J.-M., Sue, C., Walpersdorf, A., Tran, T., Lenôtre, N., Vernant, P., Cushing, M., Jouanne, F., Masson, F., Baize, S., Chéry, J., van der Beek, P.A., 2016. Present-day uplift of the western Alps. Sci. Rep. 6, 28404 https://doi.org/10.1038/srep28404.

Owen, L.A., Dortch, J.M., 2014. Nature and timing of Quaternary glaciation in the Himalayan-Tibetan orogen. Quat. Sci. Rev. 88, 14–54. https://doi.org/10.1016/j.quascirev.2013.11.016.

Pan, B., Burbank, D., Wang, Y., Wu, G., Li, J., Guan, Q., 2003. A 900 k.y. record of strath terrace formation during glacial-interglacial transitions in northwest China. Geology 31, 957–960. https://doi.org/10.1130/g19685.1.

Pardé, M., 1935. La mise en eau du barrage-réservoir du Sautet sur le Drac. Rev. Géogr. Alp. 23, 661–667. https://doi.org/10.3406/rga.1935.5481.

Penck, A., Brückner, E., 1909. Die Alpen im Eiszeitalter. Chr. Herm. Tauchnitz, Leipzig, p. 1199.

Petit, C., Goren, L., Rolland, Y., Bourlès, D., Braucher, R., Saillard, M., Cassol, D., 2017. Recent, climate-driven river incision rate fluctuations in the Mercantour crystalline massif, southern French Alps. Quat. Sci. Rev. 165, 73–87. https://doi.org/10.1016/j.quascirev.2017.04.015.

Pinter, N., Keller, E.A., West, R.B., 1994. Relative dating of terraces of the Owens River, northern California, and correlation with moraines of the Sierra Nevada. Quat. Res. 42, 266–276. https://doi.org/10.1006/qres.1994.1077.

Preusser, F., Reitner, J.M., Schlüchter, C., 2010. Distribution, geometry, age and origin of overdeepened valleys and basins in the Alps and their foreland. Swiss J. Geosci. 103, 407–426. https://doi.org/10.1007/s00015-010-0044-y.

Preusser, F., Graf, H.R., Keller, O., Krayss, E., Schlüchter, C., 2011. Quaternary glaciation history of northern Switzerland. E-G Quat. Sci. J. 60, 282–305. https://doi.org/10.3285/eg.60.2-3.06.

Roattino, T., Crouzet, C., Buoncristiani, J.F., Tissoux, H., 2021. Geometry of glaciofluvial deposits and dynamics of the Lyonnais lobe ice front during the last glacial period (France, Northern Alps). BSGF-Earth Sci. Bull. 192, 21. https://doi.org/10.1051/bsgf/2021012.

Roattino, T., Crouzet, C., Vassallo, R., Buoncristiani, J.-F., Carcaillet, J., Gribenski, N., Valla, P.G., 2023. Paleogeographical reconstruction of the western French Alps foreland during the last glacial maximum using cosmogenic exposure dating. Quat. Res. 111, 68–83. https://doi.org/10.1017/qua.2022.25.

Robert, A., 1926. La régularisation du Drac par le réservoir du Sautet. Rev. Géogr. Alp. 14–1, 219–226.

Rolland, Y., Petit, C., Saillard, M., Braucher, R., Bourlès, D., Darnault, R., Cassol, D., ASTER Team, 2017. Inner gorges incision history: a proxy for deglaciation? Insights from cosmic ray exposure dating (^{10}Be and ^{36}Cl) of river-polished surfaces (Tinée River, SW Alps, France). Earth Planet Sci. Lett. 457, 271–281. https://doi.org/10.1016/j.epsl.2016.10.007.

Schwanghart, W., Scherler, D., 2014. Short Communication: TopoToolbox 2 – MATLAB-based software for topographic analysis and modeling in Earth surface sciences. Earth Surf. Dyn. 2, 1–7. https://doi.org/10.5194/esurf-2-1-2014.

Schwartz, S., Zerathe, S., Jongmans, D., Baillet, L., Carcaillet, J., Audin, L., Dumont, T., Bourlès, D., Braucher, R., Lebrouc, V., 2017. Cosmic ray exposure dating on the large landslide of Séchilienne (Western Alps): a synthesis to constrain slope evolution. Geomorphology 278, 329–344. https://doi.org/10.1016/j.geomorph.2016.11.014.

Schwenk, M., Schläfli, P., Bandou, D., Gribenski, N., Douillet, G., Schlunegger, F., 2022. From glacial erosion to basin overfill: a 240 m-thick overdeepening-fill sequence in Bern, Switzerland. Sci. Drill. 30, 17–42. https://doi.org/10.5194/sd-30-17-2022.

Seguinot, J., Ivy-Ochs, S., Jouvet, G., Huss, M., Funk, M., Preusser, F., 2018. Modelling last glacial cycle ice dynamics in the Alps. Cryosphere 12, 3265–3285. https://doi.org/10.5194/tc-12-3265-2018.

Seguinot, J., Delaney, I., 2021. Last-glacial-cycle glacier erosion potential in the Alps, Earth Surf. Dynam 9, 923–935. https://doi.org/10.5194/esurf-9-923-2021.

Starkel, L., 2003. Climatically controlled terraces in uplifting mountain areas. Quat. Sci. Rev. 22, 2189–2198. https://doi.org/10.1016/S0277-3791(03)00148-3.

Sternai, P., Sue, C., Husson, L., Serpelloni, E., Becker, T.W., Willett, S.D., Faccenna, C., Di Giulio, A., Spada, G., Jolivet, L., Valla, P., Petit, C., Nocquet, J.-M., Walpersdorf, A., Castelltort, S., 2019. Present-day uplift of the European Alps: evaluating mechanisms and models of their relative contributions. Earth Sci. Rev. 190, 589–604. https://doi.org/10.1016/j.earscirev.2019.01.005.

Stone, J.O., 2000. Air pressure and cosmogenic isotope production. J. Geophys. Res. 105, 23753 https://doi.org/10.1029/2000JB900181.

Uppala, S.M., Kållberg, P.W., Simmons, A.J., Andrae, U., Bechtold, V.D.C., Fiorino, M., Gibson, J.K., Haseler, J., Hernandez, A., Kelly, G.A., Li, X., Onogi, K., Saarinen, S., Sokka, N., Allan, R.P., Andersson, E., Arpe, K., Balmaseda, M.A., Beljaars, A.C.M., Van De Berg, L., Bidlot, J., Bormann, N., Caires, S., Chevallier, F., Dethof, A., Dragosavac, M., Fisher, M., Fuentes, M., Hagemann, S., Holm, E., Hoskins, B.J., Isaksen, L., Janssen, P.A.E.M., Jenne, R., Mcnally, A.P., Mahfouf, J.-F., Morcrette, J.-J., Rayner, N.A., Saunders, R.W., Simon, P., Sterl, A., Trenberth, K.E., Untch, A., Vasiljevic, D., Viterbo, P., Woollen, J., 2005. The ERA-40 re-analysis. Q. J. R. Meteorol. Soc. 131, 2961–3012. https://doi.org/10.1256/qj.04.176.

Valla, P.G., van der Beek, P.A., Carcaillet, J., 2010. Dating bedrock gorge incision in the French Western Alps (Ecrin-Pelvoux massif) using cosmogenic ^{10}Be. Terra. Nova 22, 18–25. https://doi.org/10.1111/j.1365-3121.2009.00911.x.

Valla, P.G., Shuster, D.L., van der Beek, P.A., 2011. Significant increase in relief of the European Alps during mid-Pleistocene glaciations. Nat. Geosci. 4, 688–692. https://doi.org/10.1038/ngeo1242.

Valla, P.G., Sternai, P., Fox, M., 2021. How climate, uplift and erosion shaped the Alpine topography. Elements 17, 41–46. https://doi.org/10.2138/gselements.17.1.41.

Vandenberghe, J., 2008. The fluvial cycle at cold–warm–cold transitions in lowland regions: a refinement of theory. Geomorphology 98, 275–284. https://doi.org/10.1016/j.geomorph.2006.12.030.

Wallinga, J., Murray, A., Wintle, A., 2000. The single-aliquot regenerative-dose (SAR) protocol applied to coarse-grain feldspar. Radiat. Meas. 32, 529–533. https://doi.org/10.1016/S1350-4487(00)00091-3.

Wickert, A.D., Schildgen, T.F., 2019. Long-profile evolution of transport-limited gravel-bed rivers. Earth Surf. Dyn. 7, 17–43. https://doi.org/10.5194/esurf-7-17-2019.

Wintle, A.G., Murray, A.S., 2006. A review of quartz optically stimulated luminescence characteristics and their relevance in single-aliquot regeneration dating protocols. Radiat. Meas. 41, 369–391. https://doi.org/10.1016/j.radmeas.2005.11.001.

Zech, R., May, J., Kull, C., Ilgner, J., Kubik, P.W., Veit, H., 2008. Timing of the late Quaternary glaciation in the Andes from ~15 to 40° S. J. Quat. Sci. 23, 635–647. https://doi.org/10.1002/jqs.1200.